Journal Pre-proofs

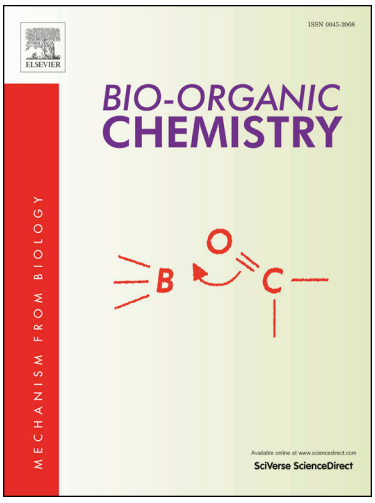


# Synthesis of furocoumarin–stilbene hybrids as potential multifunctional drugs against multiple biochemical targets associated with Alzheimer's disease

Emmanuel N. Agbo, Samantha Gildenhuys, Yee Siew Choong, Malose J. Mphahlele, Garland K. More

PII: S0045-2068(20)31294-3
DOI: https://doi.org/10.1016/j.bioorg.2020.103997
Reference: YBIOO 103997

To appear in: *Bioorganic Chemistry*

Received Date: 28 March 2020
Revised Date: 26 May 2020
Accepted Date: 2 June 2020

Please cite this article as: E.N. Agbo, S. Gildenhuys, Y. Siew Choong, M.J. Mphahlele, G.K. More, Synthesis of furocoumarin–stilbene hybrids as potential multifunctional drugs against multiple biochemical targets associated with Alzheimer's disease, *Bioorganic Chemistry* (2020), doi: https://doi.org/10.1016/j.bioorg.2020.103997

# Synthesis of furocoumarin–stilbene hybrids as potential multifunctional drugs against multiple biochemical targets associated with Alzheimer's disease

Emmanuel N. Agbo,[1] Samantha Gildenhuys,[2] Yee Siew Choong,[3] Malose J. Mphahlele[1*] and Garland K. More[2]

[1] Department of Chemistry, College of Science, Engineering and Technology, University of South Africa, Private Bag X06, Florida 1710, South Africa

[2] Department of Life & Consumer Sciences, College of Agriculture and Environmental Sciences, University of South Africa, Private Bag X06, Florida 1710, South Africa

[3] Institute for Research in Molecular Medicine (INFORMM), Universiti Sains Malaysia, Penang 11800, Malaysia

***** Author for correspondence: mphahmj@unisa.ac.za

**Abstract:** A series of furocoumarin-stilbene hybrids has been synthesized and evaluated *in vitro* for inhibitory effect against acetylcholinesterase (AChE), butyrylcholinestarase (BChE), β-secretase, cyclooxygenase-2 (COX-2), and lipoxygenase-5 (LOX-5) activities including free radical-scavenging properties. Among these hybrids, 8-(3,5-dimethoxyphenyl)-4-(3,5-dimethoxystyryl)furochromen-2-one **4h** exhibited significant anticholinesterase activity and inhibitory effect against β-secretase, COX-2 and LOX-5 activities. 2,2-Diphenyl-1-picrylhydrazyl (DPPH) radical scavenging activity and an *in vitro* cell-based antioxidant activity assay involving lipopolysaccharide induced reactive oxygen species production revealed that **4h** has capability of scavenging free radicals. Molecular docking into AChE, BChE, β-secretase, COX-2 and LOX-5 active sites has also been performed.

**Keywords:** furocoumarin–stilbene hybrids; cholinesterases; β-secretase; cyclooxygenase-2, lipoxygenase-5; antioxidant effect; molecular docking

## 1. Introduction

Alzheimer's disease (AD) is the dominant form of dementia affecting the elderly and this disease is characterized by difficulties in speaking and memory loss, and other cognitive impairments, along with changes in mood and behaviour [1]. The brains of patients suffering from AD are characterized by abnormal accumulation of β-amyloid (Aβ) plaques and the deposition of neurofibrillary tangles associated with oxidative damage [2]. Several molecular mechanisms are implicated in the pathogenesis and progression of AD including low levels of acetylcholine, formation of Aβ deposits, oxidative stress, and metal (iron, copper or zinc) imbalance [3]. Chronic inflammation is also present in the background of AD [4], and neuroinflammation represents an important pathophysiological feature and an early sign of AD [5]. Therapeutic strategies currently pursued for the treatment of AD include inhibition of cholinesterases, which is limited to four acetylcholinesterase (AChE) inhibitors, namely, donepezil, rivastigmine, galantamine and tacrine, and the targeting of Aβ peptides as well as metal-Aβ complexes [6]. A key determinant of the therapeutic properties of the central nervous system (CNS) drugs is their ability to cross the plasma membrane, and most importantly the blood–brain barrier (BBB) [7,8]. Because of its multifunctional origins, the use of cholinesterase inhibitors such as donepezil (Figure 1) to treat AD has only proven to be insufficient in slowing down or stopping completely the progression of this neurodegenerative disease [9,10]. A contemporary view supports the development of a drug agent with multiple therapeutic targets capable of simultaneously addressing two or more key pathophysiological processes linked to AD rather than single-targeted drugs [11-13]. We have previously employed this strategy on a series of 5-oxo-5*H*-furo[3,2-*g*]chromene-6-carbaldehydes of the generalized structure (**A**) shown in Figure 1 *in vitro* against several biochemical targets linked to the mechanisms that underpin the pathogenesis and progression of this disease [14].

Furocoumarins, which are analogues of furochromenones serve as photochemotherapeutic [15], antitumor [16,17], antioxidant and anti-inflammatory [18] agents, and some derivatives have also been evaluated for inhibitory effect against acetylcholinesterase (AChE) and butyrylcholinesterase (BChE) [19], and β-secretase [19] activities. The presence of a lactone moiety in the case of these benzopyran-2-one based compounds has been found to facilitate non-covalent interactions with protein residues and, in turn, promote the inhibition of cholinesterases [20]. It has also been found that furocoumarins with a higher number of $sp^2$ hybridised atoms show greater AChE inhibition potency [21]. The naturally occurring coumarins, furanocoumarins, and pyranocoumarins, on the other hand, were previously screened for inhibitory effect against β-secretase (BACE1), and only the furanocoumarins were found to exhibit activity against this enzyme [22]. The high lipophilicity and smaller sizes of furocoumarins (less than 700 Dalton) are envisioned to facilitate the crossing of the plasma membrane and BBB by these compounds, which make them suitable candidates for development into potential drugs against AD [22]. Current evidence suggests pterostilbene or *trans*-3,5-dimethoxy-4-hydroxystilbene (**B**) obtained from blue berries to be a potent modulator for age-related disease, including oxidative damage, inflammation, neurodegeneration, obesity, diabetes, and cardiovascular diseases [23]. The presence of this moiety on position-4 of the coumarin scaffold, on the other hand, has previously been found to increase the antiproliferative activity of **C**, more so than the analogous *trans*-3,5-dimethylstyryl substituted derivative **D** [24,25]. Pterostilbene inhibits the self-induced A*β*-aggregation and prevent Aβ neurotoxicity [26-29]. Low doses of this compound administered to SAMPE mice have previously been found to significantly improve their radial arm water maze (RAWM) function, which is a model for AD to measure the effects of chronic stress on memory [27]. Polymethoxystilbenes generally interact with biomembrane models, undergo a different metabolic conversion and have a higher bioavailability compared to resveratrol [30].

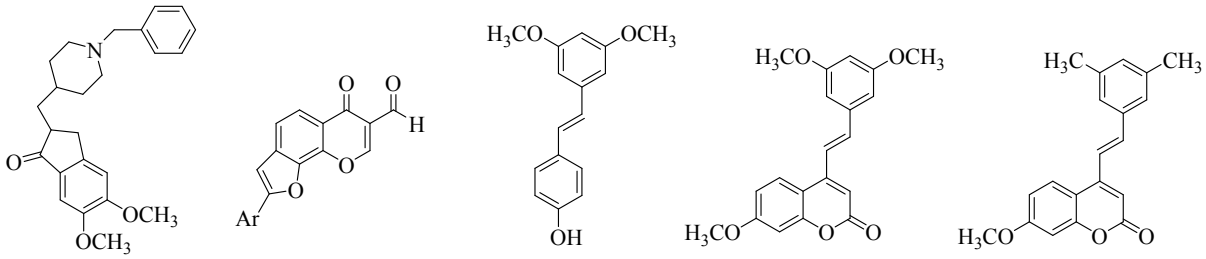

Donepezil **A** **B** **C** **D**

**Figure 1:** Structures of donepezil, furochromenones (**A**), pterostilbene (**B**) and coumarin-stilbenes (**C**) & (**D**).

We considered the therapeutic potential of furocoumarins and pterostilbene against AD, and decided to merge these two pharmacophores on the same molecular framework to construct furocoumarin-stilbene hybrids with increased inhibitory effect against cholinesterases (AChE and BChE) and β-secretase activities. Due to the multifunctional origin of AD, the prepared molecular hybrids were also evaluated for inhibitory effect *in vitro* against cyclooxygenase-2 (COX-2) and lipoxygenase-5 (LOX-5) as well as for free radical scavenging potential using the 2,2-diphenyl-1-picrylhydrazyl (DPPH) radical scavenging assay. Moreover, a cell-based antioxidant activity assay on the most active compounds involving lipopolysaccharide (LPS) induced reactive oxygen species (ROS) production in the breast MCF-7 cancer cell line and human embryonic kidney derived Hek293-T cells was performed. Kinetic and molecular docking studies of the most active derivatives have also been undertaken to rationalize their possible mode of interaction with protein residues in the active sites of AChE, BChE and β-secretase.

## 2. Materials and Methods

### 2.1. General

Commercially available materials were obtained from the suppliers and used without further purification. The melting point (mp.) values of the prepared compounds were recorded on a Thermocouple digital melting point apparatus (Mettler Toledo LLC, Columbus, OH, USA) and

are uncorrected. The IR spectra were recorded using the thin-film method on a Bruker VERTEX 70 FT-IR Spectrometer (Bruker Optics, Billerica, MA, USA) equipped with a diamond attenuated total reflectance (ATR) accessory. The Merck kieselgel 60 (0.063–0.200 mm) (Merck KGaA, Frankfurt, Germany) was employed as a stationary phase for silica gel column chromatographic purifications. The NMR ($^{1}$H- and $^{13}$C-) spectra were obtained as DMSO-$d_6$ solutions using Varian Mercury 300 MHz NMR spectrometer (Varian Inc., Palo Alto, CA, USA). The chemical shifts are quoted relative to tetramethylsilane (TMS) as an internal reference standard and the coupling constant values (*J*) are represented in Hertz (Hz). The high-resolution mass spectra were recorded at an ionization potential of 70 eV using Micromass Autospec-TOF (double focusing high resolution) instrument (Waters Corp., Milford, MA, USA).

### 2.2. Preparation of substrates

2.2.1. Synthesis of 4-(bromomethyl)-7-hydroxycoumarin

A stirred solution of 4-(bromomethyl)-7-methoxycoumarin (1.00 g, 3.72 mmol) in dichloromethane (10 mL) at 0 °C in a two-necked round bottom flask equipped with a rubber septum and a balloon containing argon gas was treated dropwise with a solution of $BBr_3$ (1.0 M in dichloromethane; 11.18 mol, 1.06 mL) by means of a syringe. The ice bath was removed, and the mixture was allowed to warm to room temperature (RT) and stirring was continued for 16 h under argon atmosphere. The mixture was poured onto crushed ice and stirred for 30 minutes. The resulting precipitate was filtered on a sintered funnel and the residue was recrystallized from ethanol to afford 4-bromomethyl-7-hydroxycoumarin as a white solid (0.83 g, 87%), mp. 188–189 ºC, $\nu_{max}$ (ATR) 725, 846, 853, 1207, 1269, 1403, 1607, 1721 (C=O), 3130, 3443 cm$^{-1}$; $\delta_H$ (300 MHz, DMSO-$d_6$) 4.80 (2H, s, -$CH_2$Br), 6.45 (1H, s, H-3), 6.74 (1H, s, H-8), 6.85 (1H, dd, $J$ = 2.0 Hz and 9.0 Hz, H-6), 7.70 (1H, d, $J$ = 9.0 Hz, H-5), 10.64 (1H, s, -OH); $\delta_C$ (75 MHz, DMSO-$d_6$) 59.4, 102.7, 106.9, 110.0, 113.3, 126.0, 155.3, 157.3, 161.1, 161.4; HRMS (ES$^+$): m/z [M + H]$^+$ calcd for $C_{10}H_8O_3{}^{79}Br$: 254.9657; found 254.9652.

2.2.2. Synthesis of 4-(bromomethyl)-7-hydroxy-8-iodocoumarin (**1**)

A stirred solution of 4-(bromomethyl)-7-hydroxycoumarin (1.00 g, 2.94 mmol) in acetic acid (10 mL) at RT was treated with *N*-iodosuccinimide (0.88 g, 2.94 mmol). The mixture was stirred at RT for 3 h and then poured into an ice-cold aqueous solution of sodium thiosulphate. The product was extracted into chloroform and the combined organic phases were washed with water, and dried using sodium sulphate. The precipitate was filtered and recrystallized from ethanol to afford **1** as a white solid (0.94 g, 84 %), mp. 213–213 ºC; $\nu_{max}$ (ATR) 807, 815, 1036, 1121, 1313, 1390, 1551, 1601, 1694 (C=O), 3057, 3395 $cm^{-1}$; $\delta_H$ (300 MHz, DMSO-$d_6$) 5.01 (2H, s, -$CH_2$Br), 6.71 (1H, s, H-3), 7.15 (1H, d, $J$ = 8.7 Hz, H-6), 7.91 (1H, d, $J$ = 8.7 Hz, H-5), 11.67 (1H, s, -OH); $\delta_C$ (75 MHz, DMSO-$d_6$) 28.2, 28.3, 75.3, 110.6, 112.1, 112.3, 126.8, 151.9, 155.3, 160.3, 161.8; HRMS ($ES^+$): m/z $[M + H]^+$ calcd for $C_{10}H_6O_3{}^{79}BrI$: 381.8692; found 381.8485.

2.2.3. Synthesis of diethyl ((7-hydroxy-8-iodo-2-oxo-2*H*-chromen-4-yl)methyl)phosphonate (**2**)

A stirred mixture of **1** (1.00 g, 2.62 mmol) and triethylphosphite (0.87 g, 5.24 mmol) was heated under reflux for 18 h. The excess triethylphospite was removed under reduced pressure using a Buchii bulb-to-bulb distillation oven. The residue was poured into crush ice and stirred for 30 minutes. The resulting precipitate was filtered and wash with cold hexane to afford the phosphonate product **2** as a white solid (0.90 g, 79%), mp. 216–217 ºC; $\nu_{max}$ (ATR) 816, 851, 1021, 1039, 1205, 1251, 1385, 1603, 1716 (C=O), 3072, 3404 $cm^{-1}$; $\delta_H$ (300 MHz, DMSO-$d_6$) 1.14 (6H, t, $J$ = 6.8 Hz, -$CH_3$), 3.50 (2H, d, $J_{HP}$ = 24.3 Hz, -$CH_2$P), 3.91–4.02 (4H, m, -$OCH_2$-), 6.21 (1H, d, $J_{HP}$ = 3.8 Hz, H-3), 6.86 (1H, d, $J$ = 8.7 Hz, H-6), 7.73 (1H, d, $J$ = 8.7 Hz, H-5), 11.40 (1H, s, -OH); $\delta_C$ (75 MHz, DMSO-$d_6$) 16.5, 16.6, 28.4, 30.2, 62.3 (d, $J$ = 6.8 Hz), 74.9, 111.6, 112.2 (d, $J$ = 4.5 Hz), 112.7 (d, $J$ = 8.0 Hz), 128.1, 149.1 (d, $J$ = 8.0 Hz), 154.9, 160.0, 161.7; $\delta_P$ (300 MHz, DMSO-$d_6$) 23.3 ppm; HRMS ($ES^+$): m/z $[M + H]^+$ calcd for $C_{14}H_{16}O_6IP$: 438.9808; found 438.9697.

2.2.4. Synthesis of (*E*)-4-(3,5-dimethoxystyryl)-7-hydroxy-8-iodo-2*H*-chromen-2-one (**3**).

A stirred solution of **2** (0.20 g, 0.44 mmol) in THF (5 mL) at -10 °C was treated with sodium hydride (0.04 g, 1.76 mmol). After 30 minutes at this temperature, the mixture was treated dropwise with a solution of 3,5-dimethoxybenzaldehyde (0.22 g, 1.32 mmol) in THF (5 mL) using a syringe. The mixture was allowed to warm to RT and stirring was continued for 6 h with thin layer chromatography (TLC) monitoring. Water (10 mL) was added to the reaction mixture and the product was extracted into chloroform. The combined organic phases were washed with brine and dried over anhydrous sodium sulphate. The salt was filtered off and the solvent was evaporated under reduced pressure on a rotary evaporator. The residue was purified by silica gel column chromatography to afford compound **3** as a brown solid (0.14 g, 72%), $R_f$ (1:3 ethyl acetate-hexane) 0.52, mp. 252–254 ºC; $\nu_{max}$ (ATR) 804, 1046, 1152, 1201, 1302, 1343, 1430, 1530, 1582, 1715 (C=O), 3020 $cm^{-1}$; $\delta_H$ (300 MHz, DMSO-$d_6$) 3.79 (6H, s, -$OCH_3$), 6.50 (1H, s, H-4′), 6.53 (1H, s, H-3), 6.93 (1H, d, $J$ = 8.7 Hz, H-6), 6.96 (2H, s, H-2′,6′), 7.50 (1H, d, $J_{trans}$ = 16.0 Hz, $H_a$), 7.62 (1H, d, $J_{trans}$ = 16.0 Hz, $H_b$), 8.02 (1H, d, $J$ = 8.7 Hz, H-5), 11.45 (1H, s, -OH); $\delta_C$ (75 MHz, DMSO-$d_6$) 55.8, 75.6, 102.1, 105.6, 106.4, 111.7, 112.0, 121.2, 127.0, 138.2, 138.5, 150.6, 155.2, 160.9, 161.1, 161.9; HRMS ($ES^+$): m/z $[M + H]^+$ calcd for $C_{10}H_6O_3{}^{79}BrI$; 451.0002; found 450.9958. Anal. Calcd for $C_{10}H_5O_3BrI$: C, 50.69; H, 3.36, Found: C, 50.70; H, 3.32.

**2.3. Typical procedure for tandem Sonogashira cross-coupling cycloisomerization of 3.**

A mixture of **3** (0.10 g, 0.22 mmol), $PdCl_2(PPh_3)_2$ (0.016 g, 0.02 mmol), CuI (0.008 g, 0.04 mmol), $Et_3N$ (0.03 g, 0.33 mmol), and triphenyl phosphine (0.006 g, 0.02 mmol) in 9:1 DMF-water (v/v, 20 mL) was placed in a two necked round-bottom flask equipped with a condenser, and rubber septum. The mixture was purged with nitrogen gas for 30 minutes and a balloon filled with nitrogen gas was connected to the top of the condenser. A solution of phenylacetylene (0.03 g, 0.30 mmol) in DMF (1 mL) was added through the rubber septum by means of a syringe. The mixture was then stirred at 70 °C for 3 h under an inert atmosphere. The mixture was poured into

an ice-cold water and the product was extracted with chloroform. The combined organic extracts were washed with brine and then dried over anhydrous magnesium sulphate. The salt was filtered off and the solvent was evaporated under reduced pressure on a rotary evaporator. The residue was purified by silica gel column chromatography using a 9:1 toluene-ethyl acetate mixture (v/v) as an eluent. Compounds **4a**–**h** were prepared in this fashion.

(*E*)-4-(3,5-Dimethoxystyryl)-8-phenyl-2*H*-furo[2,3-*h*]chromen-2-one (**4a**)

Brown solid (0.07 g, 77%), $R_f$ (toluene-ethyl acetate) 0.73, mp. 214–215 °C; $\nu_{max}$ (ATR) 792, 1054, 1142, 1211, 1323, 1362, 1410, 1591, 1610, 1698 (C=O), 3028 $cm^{-1}$; $\delta_H$ (300 MHz, DMSO-$d_6$) 3.80 (6H, s, -$OCH_3$), 6.52 (1H, s, H-4′), 6.76 (1H, s, H-3), 7.01 (2H, d, $J$ = 1.2 Hz, H-2′,6′), 7.44 (1H, d, $J$ = 7.8 Hz, H-5), 7.52 (1H, s, H-9), 7.52 (1H, d, $J_{trans}$ = 16.0 Hz, $H_a$), 7.59 (1H, d, $J_{trans}$ = 16.0 Hz, $H_b$), 7.68–7.81 (3H, m, Ar), 8.00 (2H, d, $J$ = 7.8 Hz, Ar), 8.16 (1H, d, $J$ = 9.3 Hz, H-6); $\delta_C$ (75 MHz, DMSO-$d_6$) 55.8, 99.6, 102.1, 106.4, 107.6, 108.6, 113.7, 118.5, 121.5, 122.3, 125.4, 129.5 (2xC), 129.6, 129.8, 138.2, 138.7, 147.6, 151.5, 156.8, 160.5, 161.1; HRMS ($ES^+$): $m/z$ $[M + H]^+$ calcd for $C_{27}H_{20}O_5$: 425.1389; found 425.1382. Anal. Calcd for $C_{27}H_{19}O_5$: C, 76.40; H, 4.75, Found: C, 76.35; H, 4.69.

(*E*)-4-(3,5-Dimethoxystyryl)-8-(3-fluorophenyl)-2*H*-furo[2,3-*h*]chromen-2-one (**4b**)

Brown solid (0.07 g, 74%), $R_f$ (toluene-ethyl acetate) 0.71, mp. 257–258 °C; $\nu_{max}$ (ATR) 764, 780, 796, 830, 1068, 1154, 1205, 1303, 1350, 1478, 1563, 1597, 1730 (C=O), 2924 $cm^{-1}$; $\delta_H$ (300 MHz, DMSO-$d_6$) 4.05 (6H, s, -$OCH_3$), 6.77 (1H, s, H-4′), 7.00 (1H, s, H-3), 7.24 (2H, d, $J$ = 1.8 Hz, H-2′,6′), 7.51 (1H, t, $J$ = 8.4 Hz, H-4″), 7.81 (2H, dd, $J_{HH}$ = 7.5 Hz and $J_{HF}$ = 9.9 Hz, H-2″,5″), 7.93 (1H, d, $J$ = 9.0 Hz, H-5), 8.00 (1H, d, $J_{trans}$ = 15.5 Hz, $H_a$), 8.04 (1H, d, $J_{trans}$ = 15.5 Hz, $H_b$), 8.07 (1H, d, $J$ = 7.8 Hz, H-2″), 8.17 (1H, s, H-9), 8.43 (1H, d, $J$ = 9.3 Hz, H-6); $\delta_C$ (75 MHz, DMSO-$d_6$) 55.6, 56.0, 98.8, 100.8, 101.0, 106.6, 107.2, 107.9, 108.4, 108.8, 112.0, 112.4, 114.0, 116.5 (d, $^2J_{CF}$ = 21.75 Hz), 121.5 (d, $^4J_{CF}$ = 2.87 Hz), 123.0 (d, $^3J_{CF}$ = 12.25Hz), 131.3 (d, $^3J_{CF}$ = 10.28 Hz), 138.3, 138.8, 141.7, 147.3, 155.8, 156.3 (d, $^2J_{CF}$ = 21.75 Hz), 160.0, 163.2 (d,

$^{1}J_{CF}$ = 246.5 Hz); HRMS (ES$^{+}$): *m*/*z* [M + H]$^{+}$ calcd for $C_{27}H_{19}O_5F$: 443.1295; found 443.1281. Anal. Calcd for $C_{27}H_{18}O_5F$: C, 73.30; H, 4.33, Found: C, 73.30; H, 4.31.

(*E*)-4-(3,5-Dimethoxystyryl)-8-(4-fluorophenyl)-2*H*-furo[2,3-*h*]chromen-2-one (**4c**)

Yellow solid (0.08 g, 79%), $R_f$ (toluene-ethyl acetate) 0.64, mp. 243–244 °C; $\nu_{max}$ (ATR) 763, 797, 828, 1058, 1067, 1149, 1186, 1302, 1348, 1455, 1564, 1592, 1725 (C=O), 2924 cm$^{-1}$; $\delta_H$ (300 MHz, DMSO-$d_6$) 4.04 (6H, s, -$OCH_3$), 6.78 (1H, s, H-4′), 6.98 (1H, s, H-3), 7.26 (2H, d, *J* = 1.8 Hz, H-2′,6′), 7.61 (2H, t, $J_{HH}$ = 8.7 Hz, H-2″,6″), 7.80 (1H, d, $J_{trans}$ = 15.5 Hz, $H_a$), 7.92 (1H, d, *J* = 8.7 Hz, H-5), 8.00 (1H, d, $J_{trans}$ = 15.5 Hz, $H_b$), 8.03 (1H, s, H-9), 8.28 (2H, dt, $J_{HH}$ = 8.7 Hz and $J_{HF}$ = 5.7 Hz, H-3″,5″), 8.40 (1H, d, *J* = 9.0 Hz, H-6); $\delta_C$ (75 MHz, DMSO-$d_6$) 56.1, 99.7, 102.4, 106.7, 107.9, 108.8, 110.0, 114.0, 116.9 (d, $^{2}J_{CF}$ = 22.8 Hz), 118.8, 121.8, 122.6, 126.4 (d, $^{4}J_{CF}$ = 3.5 Hz), 127.9 (d, $^{3}J_{CF}$ = 9.1 Hz), 138.4, 138.9, 148.1, 151.7, 156.2, 157.0, 160.7, 163.2 (d, $^{1}J_{CF}$ = 64.5 Hz); HRMS (ES$^{+}$): m/z [M + H]$^{+}$ calcd for $C_{27}H_{19}O_5F$: 443.1295; found 443.1284. Anal. Calcd for $C_{27}H_{18}O_5F$: C, 73.30; H, 4.33. Found: C, 73.32; H, 4.29.

(*E*)-4-(3,5-Dimethoxystyryl)-8-(3-chlorophenyl)-2*H*-furo[2,3-*h*]chromen-2-one (**4d**)

Yellow solid (0.07 g, 69%), $R_f$ (toluene-ethyl acetate) 0.65, mp. 263–264 °C; $\nu_{max}$ (ATR) 495, 670, 795, 1044, 1168, 1217, 1325, 1359, 1411, 1598, 1607, 1738 (C=O), 3017 cm$^{-1}$; $\delta_H$ (300 MHz, DMSO-$d_6$) 4.05 (6H, s, -$OCH_3$), 6.80 (1H, s, H-4′), 7.02 (1H, s, H-3), 7.27 (2H, d, *J* = 1.8 Hz, H-2′,6′), 7.74–7.82 (3H, m, Ar), 7.86 (1H, d, $J_{trans}$ = 16.0 Hz, $H_a$), 7.98 (1H, d, *J* = 8.7 Hz, H-5), 8.00 (1H, d, $J_{trans}$ = 16.0 Hz, $H_b$), 8.22 (1H, s, Ar), 8.32 (1H, s, H-9), 8.45 (1H, d, *J* = 8.7 Hz, H-6); $\delta_C$ (75 MHz, DMSO-$d_6$) 55.7, 56.1, 101.1, 106.7, 107.4, 108.5, 110.0, 112.2, 114.1, 118.2, 124.1, 125.1, 129.7, 131.6, 131.7, 134.6, 134.7, 141.8, 147.5, 155.3, 155.9, 156.8, 160.2, 160.8, 161.4; HRMS (ES$^{+}$): *m*/*z* [M + H]$^{+}$ calcd for $C_{27}H_{19}O_5{}^{35}Cl$: 459.0999; found 459.0997. Anal. Calcd for $C_{27}H_{18}O_5Cl$: C, 70.67; H, 4.17, Found: C, 70.63; H, 4.18.

(*E*)-4-(3,5-Dimethoxystyryl)-8-(4-chlorophenyl)-2*H*-furo[2,3-*h*]chromen-2-one (**4e**)

Brown solid (0.06 g, 60%), $R_f$ (toluene-ethyl acetate) 0.68, mp. 230–231 °C; $\nu_{max}$ (ATR) 511, 652, 792, 1112, 1162, 1219, 1223, 1352, 1413, 1585, 1612, 1729 (C=O), 3001 $cm^{-1}$; $\delta_H$ (300 MHz, DMSO-$d_6$) 4.05 (6H, s, -$OCH_3$), 6.80 (1H, t, $J$ = 2.4 Hz, H-4′), 6.98 (1H, s, H-3), 7.25 (2H, d, $J$ = 2.4 Hz, H-2′,6′), 7.80 (2H, d, $J$ = 8.7 Hz, H-3″,5″), 7.82 (1H, d, $J_{trans}$ = 15.5 Hz, $H_b$), 7.90 (1H, d, $J$ = 8.7 Hz, H-5), 8.00 (1H, d, $J_{trans}$ = 15.5 Hz, $H_b$), 8.10 (1H, s, H-9), 8.24 (2H, d, $J$ = 8.7 Hz, H-2″,6″), 8.35 (1H, d, $J$ = 9.0 Hz, H-6); $\delta_C$ (75 MHz, DMSO-$d_6$) 55.1 (2×C), 99.5, 101.4, 105.7, 106.9, 107.8, 113.0, 117.7, 120.7, 121.8, 126.3, 127.6, 128.9, 133.5, 137.4, 137.9, 147.1, 150.6, 154.8, 156.0, 159.7, 160.4; HRMS ($ES^+$): $m/z$ $[M + H]^+$ calcd for $C_{27}H_{19}O_5{}^{35}Cl$: 459.0999; found 459.0987. Anal. Calcd for $C_{27}H_{18}O_5Cl$: C, 70.67; H, 4.17, Found: C, 70.59; H, 4.16.

(*E*)-4-(3,5-Dimethoxystyryl)-8-(*p*-tolyl)-2*H*-furo[2,3-*h*]chromen-2-one (**4f**)

Brown solid (0.07 g, 69%), $R_f$ (toluene-ethyl acetate) 0.60, mp. 206–207 °C; $\nu_{max}$ (ATR) 501, 650, 790, 1111, 1166, 1212, 1220, 1355, 1423, 1578, 1610, 17.34 (C=O), 3008 $cm^{-1}$; $\delta_H$ (300 MHz, DMSO-$d_6$) 2.60 (3H, s, -$CH_3$), 4.02 (6H, s, -$OCH_3$), 6.77 (1H, t, $J$ = 2.4 Hz, H-4′), 6.98 (1H, s, H-3), 7.23 (2H, d, $J$ = 2.1 Hz, H-2′,6′), 7.56 (2H, d, $J$ = 8.4 Hz, H-3″,5″), 7.83 (1H, d, $J_{trans}$ = 16.5 Hz, $H_a$), 7.92 (1H, d, $J$ = 9.0 Hz, H-5), 7.96 (1H, s, H-9), 8.00 (1H, d, $J_{trans}$ = 16.5 Hz, $H_b$), 8.12 (2H, d, $J$ = 7.5 Hz, H-2″,6″), 8.37 (1H, d, $J$ = 8.7 Hz, H-6); $\delta_C$ (75 MHz, DMSO-$d_6$) 22.1, 56.5 (2×C), 99.4, 102.8, 107.1, 108.3, 109.1, 114.3, 119.2, 122.2, 122.7, 126.0, 127.4, 130.8, 138.8, 139.3, 140.2, 148.4, 152.1, 157.3, 157.7, 161.2, 161.8, 161.9; HRMS ($ES^+$): $m/z$ $[M + H]^+$ calc. for $C_{28}H_{22}O_5$: 439.1546; found 439.1541. Anal. Calcd for $C_{28}H_{21}O_5$: C, 76.70; H, 5.06, Found: C, 76.67; H, 5.03.

(*E*)-4-(3,5-Dimethoxystyryl)-8-(4-methoxyphenyl)-2*H*-furo[2,3-*h*]chromen-2-one (**4g**)

Brown solid (0.07 g, 72%), $R_f$ (toluene-ethyl acetate) 0.56, mp. 222–223 °C; $\nu_{max}$ (ATR) 479, 648, 788, 1102, 1165, 1222, 1231, 1354, 1416, 1581, 1616, 1720 (C=O), 3000 $cm^{-1}$; $\delta_H$ (300 MHz, DMSO-$d_6$) 4.05 (9H, s, -$OCH_3$), 6.77 (1H, t, $J$ = 2.4 Hz, H-4′), 6.97 (1H, s, H-3), 7.25 (2H, d, $J$ = 2.4 Hz, H-2′,6′), 7.31 (2H, d, $J$ = 8.7 Hz, H-3″,5″), 7.73 (1H, d, $J_{trans}$ = 16.0 Hz, $H_a$), 7.86

(1H, s, H-9), 7.90 (1H, d, $J$ = 9.0 Hz, H-5), 8.00 (1H, d, $J_{trans}$ = 16.0 Hz, $H_b$), 8.14 (2H, d, $J$ = 8.7 Hz, H-2″,6″), 8.34 (1H, d, $J$ = 9.0 Hz, H-6); $\delta_C$ (75 MHz, DMSO-$d_6$) 55.3, 55.4 (2×C), 97.2, 101.7, 106.0, 107.1, 108.0, 113.2, 114.6, 118.3, 121.2, 121.6, 126.6, 137.7, 138.1, 140.0, 147.2, 151.1, 156.2, 156.6, 160.2.1, 160.2, 161.0; HRMS ($ES^+$): $m/z$ $[M + H]^+$ calc. for $C_{28}H_{22}O_6$: 455.1495; found 455.1487. Anal. Calcd for $C_{28}H_{22}O_6$: C, 74.00; H, 4.88, Found: C, 73.98; H, 4.85.

(*E*)-8-(3,5-Dimethoxyphenyl)-4-(3,5-dimethoxystyryl)-2*H*-furo[2,3-*h*]chromen-2-one (**4h**)

Yellow solid (0.08 g, 75%), $R_f$ (toluene-ethyl acetate) 0.52, mp. 249–250 °C; $\nu_{max}$ (ATR) 482, 655, 790, 1109, 1178, 1200, 1331, 1357, 1425, 1587, 1621, 1733 (C=O), 3010 $cm^{-1}$; $\delta_H$ (300 MHz, DMSO-$d_6$) 4.04 (6H, s, $-OCH_3$), 4.06 (6H, s, $-OCH_3$), 6.76 (2H, dt, $J$ = 2.4 Hz, H-4′,4″), 6.95 (1H, s, H-3), 7.23 (2H, d, $J$ = 2.4 Hz, H-2′,6′), 7.35 (2H, d, $J$ = 2.4 Hz, H-2″,6″), 7.79 (1H, d, $J_{trans}$ = 15.9 Hz, $H_a$), 7.89 (1H, d, $J$ = 9.0 Hz, H-5), 8.00 (1H, d, $J_{trans}$ = 15.9 Hz, $H_b$), 8.09 (1H, s, H-9), 8.35 (1H, d, $J$ = 9.0 Hz, H-6); $\delta_C$ (75 MHz, DMSO-$d_6$) 56.0 (2×C), 56.1 (2×C), 100.5, 102.4, 103.4, 106.7, 107.8, 108.8, 113.9, 118.7, 121.7, 122.6, 131.5, 138.4, 138.8, 148.1, 151.6, 156.8, 156.9, 160.7, 161.4, 161.6; HRMS ($ES^+$): $m/z$ $[M + H]^+$ calc. for $C_{28}H_{24}O_7$: 485.1600; found 485.1595. Anal. Calcd for $C_{29}H_{24}O_7$: C, 71.89; H, 4.99, Found: C, 71.91; H, 4.96.

2.4. *Biological activity studies*.

2.4.1. Cholinesterase enzyme assays of **3** and **4a**–**h**.

Cholinesterase activities were determined following a modification of the Ellman's method [33] as described in our previous study [14]. Solutions (200 μM) of the test compounds and the reference standards (donepezil and galantamine) were prepared in DMSO (20 mL) and diluted with 50 mM tris buffer (pH 7.7) to the final concentrations of 0.1, 1.0, 5, 10, 25, 50, and 100 μM, respectively. Reactions were performed in triplicate at 37 °C in a 96-well plate. To each well were added sequentially, 9.0 μL solution of the test compound, 1.0 μL of the respective enzyme, and 70 μL of tris buffer ($C_4H_{11}NO_3$, 50 mM, pH 7.7). The assay mixture was preincubated for

30 min at RT, and then 10 µL of 5,5′-dithiobis-(2-nitrobenzoic acid) (DTNB, 3 mM in tris buffer, 50 mM, pH 7.7) and 10 µL of AChI (5 mM in tris buffer, 50 mM, pH 7.7) were added sequentially to each well. Five different absorbance readings were recorded for each triplicate run at a wavelength of 412 nm [14] using a Varioskan flash spectrophotometer plate reader (Thermo Scientific, Waltham, MA, USA). The average values obtained from the absorbance readings were used to determine the $IC_{50}$ and standard deviation values using the Graph Pad Prism.

2.4.2. β-Secretase assays of compounds **3** and **4a**–**h**

The β-secretase inhibitory activities of the test compounds were assayed using a recombinant baculovirus-expressed β-secretase and a specific substrate (Rh-EVNLDAEFK-Quencher) according to the manufacturer's (Pan Vera Corp., Madison, Wisconsin, USA) instructions. Stock solution (200 µM) of the test compounds and reference standard (quercetin) were prepared in DMSO, respectively. A mixture of human recombinant BACE-1 (1.0 U/mL), the substrate (75 µM in 50 mM ammonium bicarbonate), and test compounds as well as quercetin at various concentrations (0.1, 1.0, 5, 10, 25, 50, and 100 µM) were dissolved in an assay buffer (50 mM sodium acetate buffer, pH 4.5) and then incubated for 60 minutes at 25 °C in a 96-well plate. Thereafter, 10 µL of 2.5 M sodium acetate was added to each well to stop the reactions. The increase in fluorescence intensity was observed at an emission wavelength of 590 nm on a fluorescence microplate reader (excitation wavelength = 545 nm) [14]. Five different fluorescence readings were recorded for each triplicate run and the average values obtained from the readings were used to determine the $IC_{50}$ and standard deviation values.

2.4.3. COX-2 assay for compounds **3** and **4a**–**h**

The COX-2 assay reagents were prepared according to the manufacturer (Bio Vision, Milpitas Blvd, Milpitas, CA USA) protocol enclosed in the Cyclooxygenase inhibitor screening kit (Item No. K547). Stock solutions (200 µM) of the test compounds and the standard (celecoxib) were prepared in DMSO and then diluted with tris buffer (50 Mm, pH 7.7) to obtain

final assay concentrations of 0.001, 0.01, 0.1, 1.0, 5, and 10 μM. The assays were performed in triplicates in a 96-well plate. The assay mixtures were allocated in a 96-well plate as follows: two wells for the enzyme control (10μL assay buffer) and two wells for the inhibitor control (2 μL of celecoxib and 8 μL of COX assay buffer). The test compounds concentrations (10 μL) and those of celecoxib were then added to the remaining wells. Then, 80 μL of the reaction mixture (a mixture of 76 μL COX assay buffer, 1 μL of COX probe, 2 μL of diluted COX cofactor and 1 μL of COX-2 enzyme) were added to these wells. The reaction mixtures were incubated for 5 minutes followed by addition to each well, 10 μL of diluted arachidonic acid and 90 μL of aqueous sodium hydroxide solution to initiate the reaction. Five different absorbance readings were recorded for each duplicate reaction using a Varioskan flash spectrophotometer plate reader. The average values obtained from the absorbance readings were used to determine the $IC_{50}$ and standard deviation values using the Graph Pad.

2.4.4. Human LOX-5 inhibitory assay of compounds **3** and **4a**–**h**

The reagents were prepared according to the Lipoxygenase inhibitor screening kit (Item No. K980; BioVision, Milpitas Blvd, Milpitas, CA, USA) standard protocol. Stock solutions of the test compounds were prepared in DMSO, and further diluted with 50 mM Tris HCl buffer (pH 7.7) to obtain final concentrations of 0.01, 0.1, 0.5, 1, 5, 10 and 100 μM. The reference standards, zileuton, and each compound were tested in duplicate for this assay. The composition and arrangement of the wells of a 96-well plate are as follows: two wells were blanks (40 μL of assay buffer only), two wells as enzyme controls (2 μL of LOX-5 standard and 38 μL of tris buffer), and the other two as inhibitor control (2 μL of zileuton). 2 μL of various concentration of the test compounds and reference standard, respectively, were placed in the 96 well plates followed by addition of 38 μL of LOX assay buffer to the other wells in duplicate. The reaction mixture (40 μL) prepared by mixing thoroughly 36 μL of LOX assay buffer, 2 μL of LOX probe, and 2 μL of LOX-5 enzyme was added to wells containing the test mixtures. The plate was then incubated

at 25 °C for 10 min and the reaction was initiated by addition of 20 µL of LOX substrate solution, which was prepared by diluting LOX substrate in a ratio 1:25 with assay buffer. Five absorbance readings were recorded at 234 nm using a Varioskan flash microplate spectrophotometer reader. The average values obtained from the absorbance readings were used to determine the $IC_{50}$ and standard deviation values.

2.4.5. DPPH radical scavenging activity assay of **3** and **4a**–**h**

The DPPH radical scavenging activity of compounds **3** and **4a**–**h** was evaluated by following a literature method [34] described in our previous study [14]. Briefly the test compounds and Ascorbic acid (Sigma Aldrich, Saint Louis, Missouri, USA) at various concentrations (ranging from 0 µM to 40 µM) in DMSO were mixed with a solution of DPPH (0.20 mM) in methanol and incubated in the dark for 45 min. Five absorbance readings were recorded at 512 nm using Varioskan flash microplate spectrophotometer reader. The average values obtained from the absorbance readings were used to determine the $IC_{50}$ and standard deviation values.

2.5. Evaluation of cytotoxicity (MTT assay) of **4c** and **4h** on MCF-7 and Hek293-T cells

The cytotoxic effect of compounds **4c** and **4h** on the MCF-7 and Hek293-T cells was evaluated done following a modified method by Mosmann [35]. Stock solutions (50 µM) of the test compounds and doxorubicin (positive control) were prepared in DMSO. 100 µL of HEK293-T or MCF-7 cells were grown in Dulbecco's Modified Eagle's Medium (DMEM) supplemented with 10% fetal bovine serum (FBS) and 1% penicillin-streptomycin solution. The cell cultures were seeded at a cell density of $1 \times 10^4$ cells/well in a 96 well plate. The cultures were incubated for 24 h at 37 °C under 5% $CO_2$ to allow cell growth and attachment prior treatment. After incubation, the media was aspirated, and cells were treated for 24 hours with different concentrations (0.2–25 µM) of compounds **4c** and **4h,** and doxorubicin used as a positive control. Untreated cells were used as a negative control. 100 µL of 3-(4,5-dimethylthiazol-2-Yl)-2,5-diphenyltetrazolium bromide (MTT) solution (0.5 mg/mL) was added to the cells and incubation

was continued for 3 hours. Thereafter, 100 µL DMSO was added to dissolve the formazan crystals for an hour. The plates were read at 570 nm at a reference wavelength of 630 nm using an ELISA plate reader (Varioskan Flash, ThermoFisher Scientific, Finland). The percentage of cell viability was calculated using the following formula,

$$(\%)\ \text{cell viability} = \frac{\text{At} - \text{Ab}}{\text{Ac} - \text{Ab}} \times 100$$

where, At represents Absorbance value of test compound, Ab the Absorbance value of blank and Ac the Absorbance value of control. The $IC_{50}$ values, i.e., the concentration of the drug that inhibits 50% of the cells were obtained from dose–response curves.

2.6. Measurement of intracellular LPS-induced ROS production

Determination of LPS-induced ROS production in MCF-7 and HEK293 cells was performed by measuring the oxidation of the fluorescent dye, 2′,7′-dichlorofluorescein diacetate ($H_2$DCF-DA; Sigma-Aldrich, St. Louis, Missouri, USA) [36]. Cells were seeded in 96-well plates ($1 \times 10^4$ cells/well) and incubated for 24 h at 37 $^0$C under 5% $CO_2$ prior treatment. After 24 h, the cells were treated with the test compounds (1 µM) and incubated for 1 h. The cells were further stimulated with LPS (1 µg/mL). After 6 h incubation the cells were exposed to 10 µM H2DF-DA dye and incubated for 1 h in the dark [37]. The fluorescence intensity of the cells was measured using a microplate reader (Varioskan Flash, Thermofisher Scientific, Finland). at 485 nm and 535 nm excitation and emission, respectively.

2.7. Kinetic studies of **4c** and **4h** on AChE, BChE and β-secretase

2.7.1. Kinetic studies of **4c** and **4h** on AChE and BChE

Compounds **4c** and **4h** were evaluated against AChE and BChE following a method described in our previous study [14]. Various concentrations of test compounds (0, 2.5, 3.5 and 5 µM) were used for the kinetic analysis. The Lineweaver–Burk plots (plots of the inverse of velocity against the inverse of the substrate concentration) were constructed to assess changes in

enzymatic parameters. The Dixon plots were also prepared primarily to determine the inhibitory constants ($K_i$). These plots represent an inverse of velocity (1/v) plotted against the concentration of the inhibitor at each concentration of substrate (0.1, 0.5, 2.5, 5 mM).

2.7.2. Kinetic studies of **4c** and **4h** on β-secretase

Compounds **4c** and **4h** were subjected to kinetic studies using substrate concentrations 150, 300, and 450 nM at increasing inhibitor concentrations (0, 4, 8, and 16 μM) for β-secretase. In order to establish the mode of inhibition of these compounds, the Lineweaver–Burk plots (plot of the inverse of velocity (1/v) against the inverse of the substrate concentration (1/[S])) were constructed. Dixon plots (plot of 1/v against concentration of inhibitor at each concentration of substrate) were used to determine the inhibitor constant, $K_i$.

2.8. Molecular modeling of test compounds

2.8.1. Protein setup

The starting coordinates of AChE, BChE, BACE-1, COX-2, COX-1 and LOX5 were obtained from RCSB PDB with ID 6O4W, 4BDS, 6UVP, 5IRK, 4O1Z and 3O8Y, respectively. All heteroatoms and water molecules were removed. The polar hydrogen atoms, Kollman-Amber united atom partial charges and solvation parameters were added using AutoDockTools [38].

2.8.2. Ligand setup

The starting coordinates of test compounds were prepared using Avogadro [39]. The polar hydrogen atoms were retained while the Gasteiger charges and trosional angles were assigned by AutoDockTools.

2.8.3. Docking simulation

The grid box with 50 x 50 x 50 points and 0.375 Å as grid spacing was centered protein active site. A total of 100 docking runs was performed using AutoDock4.2.6 [38] with Larmackian genetic algorithm, 2 500 000 energy evaluation, 27 000 maximum generation, 150 population, 0.02 mutation rate and 0.8 crossover rate were employed. The ligand in the most

populated cluster with most favourable binding free energy was used for further interaction analysis.

2.8.4. Pharmacokinetics properties prediction

The absorption, distribution, metabolism and excretion (ADME) values of compounds **4c** and **4h** were predicted using Molinspiration property calculation service (www.molinspiration.com). The BBB property was calculated using web based server (https://www.cbligand.org/BBB/).

## 3. Results and Discussion

### 3.1. Chemistry

The molecular construct of our potential multifunctional ligands was designed following a molecular hybridization approach as represented in Scheme 1 below and copies of their $^{1}$H- and $^{13}$C-NMR spectra are included as Figure S1 in the Supplementary Information (SI). Initial demethylation of commercially available 4-(bromomethyl)-7-methoxycoumarin with boron tribromide in dichloromethane under argon atmosphere followed by site-selective halogenation of the intermediate 4-(bromomethyl)-7-hydroxycoumarin with *N*-iodosuccinimide in acetic acid at room temperature for 3 h afforded 4-(bromomethyl)-7-hydroxy-8-iodocoumarin (**1**). The molecular framework of this compound comprises several reactive centres for further chemical transformation, *viz.*, the electrophilic methylene group for possible nucleophilic displacement of Br and the *ortho*-hydroxyiodo moiety for possible metal catalyzed cross-coupling and subsequent heteroannulation. With these considerations in mind, compound **1** was subjected to the Arbuzov reaction with triethyl phosphite under reflux for 18 h to afford a product characterised using a combination of NMR ($^{1}$H-, $^{13}$C- & $^{31}$P-), infrared and mass spectrometric techniques as diethyl ((7-hydroxy-8-iodo-2-oxo-2*H*-chromen-4-yl)methyl)phosphonate (**2**). The presence of the acidic protons of the methylenephosphonate moiety facilitated Horner-Emmons olefination of **2** with

3,5-dimethoxybenzaldehyde in the presence of sodium hydride in tetrahydrofuran (THF) at -10 °C to room temperature for 6 h. Aqueous work-up and purification by column chromatography on silica gel afforded the (*E*)-4-(3,5-dimethoxystyryl)-7-hydroxy-8-iodo-2*H*-chromen-2-one **3** in 72% yield. The $^{1}$H-NMR spectra of this compound revealed the presence of a set of doublets at δ 7.50 ppm and δ 7.62 ppm with coupling constant values $J$ = 16.0 Hz typical for the *trans*-geometry about the carbon–carbon double bond. The analogous 7-methoxycoumarins bearing a 3,5-disubstituted *trans*-vinylbenzene moiety at the C-4 position have previously been found to exhibit increased antiproliferative activity endowed with apoptosis inducing capability [25,26]. The proximity of the Csp$^{2}$–I bond to the nucleophilic hydroxyl group was exploited to facilitate palladium catalysed tandem Sonogashira cross-coupling and subsequent Cacchi-type cycloisomerization of **3** with terminal acetylenes. Aqueous work-up followed by purification using silica gel column chromatography afforded the corresponding novel furocoumarin derivatives **4a**–**h**. These tricyclic stilbene-appended molecular hybrids were easily distinguished from the corresponding substrate by the presence of increased number of signals in the aromatic region of their $^{1}$H- and $^{13}$C-NMR spectra. Their $^{13}$C-NMR spectra showed no presence of a set of carbon singlets for the acetylene moiety in the region δ 80–100 ppm, thus ruling out the possibility of the 8-alkynylated intermediates.

The presence of a hydrogen bonding lactone moiety and increased number of sp$^{2}$ hybridized atoms of the planar aromatic scaffolds of the molecular hybrids **3** and **4a**–**h** for possible protein-ligand interaction encouraged us to evaluate these compounds for inhibitory effect *in vitro* against cholinesterases and several other biochemical targets linked to the pathogenesis and progression of AD as described in the next sections.

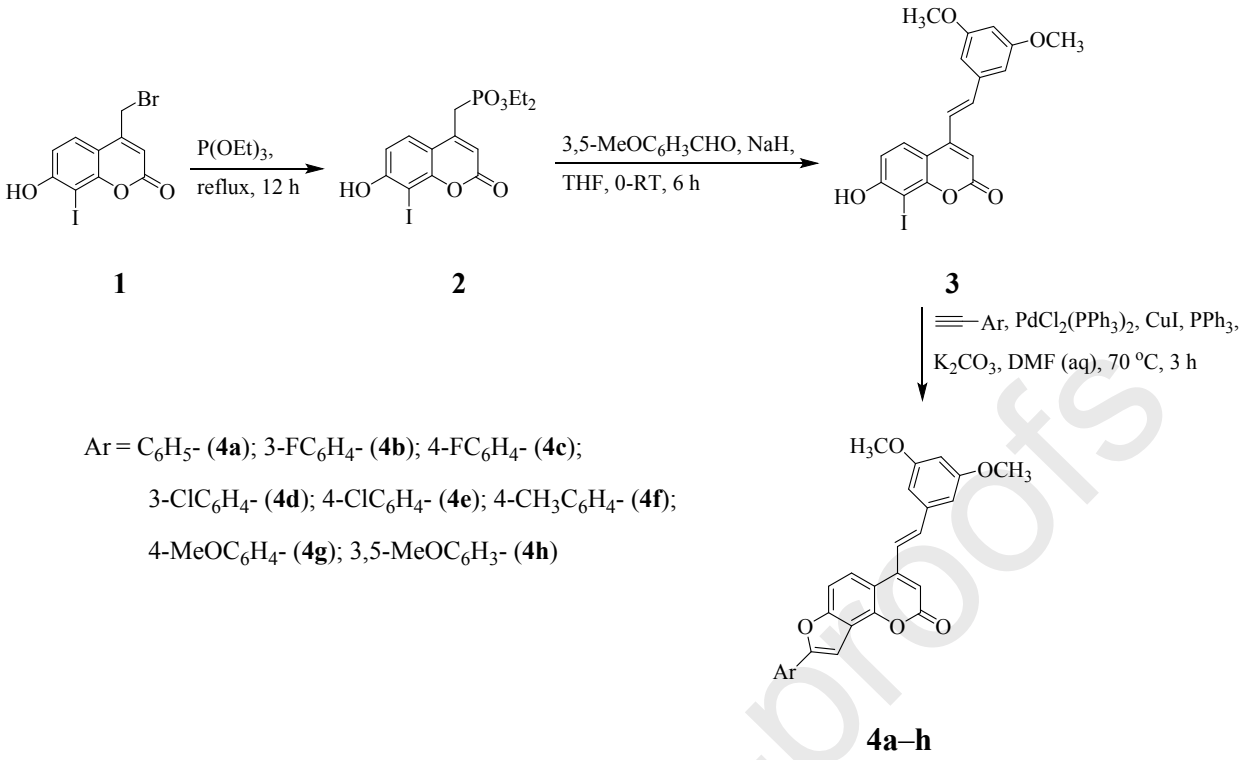


**1** **2** **3** **4a–h**

**Scheme 1**: Sequential Arbuzov and Horner-Emmons reactions as well as tandem Sonogashira cross-coupling & cycloisomerization of **3** to afford **4a–h**.

3.2. Biology

3.2.1. Cholinesterase and β-secretase inhibitory activities of compounds **3** and **4a–h**

Cholinesterase inhibitors, which will improve cognitive function and reduce the neuropathological features in AD are of great interest from medicinal point of view especially in the effective management of AD [40]. Coumarins are known to be well accommodated into the peripheral anionic site (PAS) of AChE, due to their planarity, steric complementarity, and possible π–π interactions with the aromatic residues located within this enzyme site [41]. We envisaged that the polynuclear scaffold of **4a–h** would interact with PAS and the 3,5-dimethoxyphenylstyryl arm with CAS of AChE. With these considerations in mind, compound **3** and its derivatives **4a–h** were evaluated for inhibitory potential against AChE and BChE activities using donepezil and galantamine as reference standards for the assays (Table 1). Moderate anticholinesterase activity was observed for the *ortho*-hydroxyiodo substituted coumarin-stilbene **3** with $IC_{50}$ values of 12.3 μM and 9.6 μM against AChE and BChE,

respectively. Annulation of a furan ring onto the coumarin-stilbene scaffold, on the other hand, resulted in improved and variable degree of activity for the corresponding furocoumarin-stilbene hybrids **4a**–**h** compared to the reference standards donepezil ($IC_{50}$ = 0.004 and 3.13 $\mu$M, respectively) and galantamine ($IC_{50}$ = 1.17 and 2.05 $\mu$M, respectively) with $IC_{50}$ values ranging from 1.8–21.6 $\mu$M (AChE) and 3.5–17.6 $\mu$M (BChE). The analogous 5-oxo-5*H*-furo[3,2-*g*]chromene-6-carbaldehydes were previously found to exhibit less or no activity against AChE and to exhibit moderate inhibitory effect against BChE [14]. The 8-phenyl furocoumarin–stilbene derivative **4a** exhibited relatively higher inhibitory effect than the precursor **3** against AChE and BChE with $IC_{50}$ values of 10.7 $\mu$M and 8.3 $\mu$M, respectively. The 8-(3-fluorophenyl) substituted derivative **4b** was found to be less active against AChE ($IC_{50}$ = 11.6 $\mu$M) and BChE ($IC_{50}$ = 9.1 $\mu$M) compared to the 8-(4-fluorophenyl) substituted isomer **4c** with $IC_{50}$ values of 1.8 $\mu$M (AChE) and 3.5 $\mu$M (BChE). Significantly reduced inhibition was also observed for the 8-(3-chlorophenyl) substituted derivative **4d** against AChE ($IC_{50}$ = 21.6 $\mu$M) and BChE ($IC_{50}$ = 17.6 $\mu$M). However, the corresponding 8-(4-chlorophenyl) substituted isomer **4e** exhibited significant inhibitory effect against AChE and BChE with $IC_{50}$ values of 1.9 $\mu$M and 5.3 $\mu$M, respectively. Enhanced inhibitory effect due to halogen substituents has previously been observed in series of AChE inhibitors and this observation was explained in terms of additional hydrogen bonding or dipole-dipole interactions, and/or increased van der Waals interactions [42]. The observed enhanced activity of **4b** and **4e** against the cholinesterase enzymes is presumably due to the presence of the moderately π-electron delocalizing fluorine or chlorine atom on the *para* position of the phenyl ring. π-Electron delocalizing by the 4-fluorophenyl and 4-chlorophenyl groups presumably increases the electron density of the furocoumarin scaffold and together with the 3,4-dimethoxystyryl moiety facilitate non-covalent interactions of these compounds with protein residues in PAS and/or CAS of AChE and BChE. The difference in inhibitory effect of **4c** and **4e** against both enzymes, on the other hand, is consistent with the propensity of the 4-

halogenophenyl substituted ring for π-electron delocalization (4-fluorophenyl > 4-chlorophenyl) into conjugated molecular frameworks. The presence of the more polar lipophilic 4-methoxyphenyl group at the 8-position of the furocoumarin framework of **4g** resulted in significant activity against AChE ($IC_{50}$ = 3.2 $\mu$M) and BChE ($IC_{50}$ = 4.5 $\mu$M) when compared to **4f** substituted at the *para* position of the 8-phenyl ring with a non-polar methyl group with $IC_{50}$ values of 7.5 $\mu$M and 13.8 $\mu$M, respectively. The presence of an electron rich 3,5-dimethoxyphenyl group on position-8 of the molecular framework of **4h**, on the other hand, resulted in higher activity against AChE ($IC_{50}$ = 2.8 $\mu$M) compared to **4g**. However, **4h** was comparatively less inhibiting against BChE activity with an $IC_{50}$ value of 6.3 $\mu$M, presumably due to the presence of a relatively bulky 3,5-dimethoxyphenyl ring. The ligand binding pocket of AChE consists of a long and narrow dumbbell-shaped channel extending from the surface to the interior, and the opening and bottom of this channel are relatively open, while the middle is narrow [43]. The peripheral anionic site (PAS) of AChE, which is the binding site for the enzyme inhibitors is situated at the opening of the channel. It is envisaged that the relatively bulky electron rich **4h** would fit well into the large active site cleft of AChE to engage in non-covalent interactions with the receptor. The larger size of the 3,5-dimethoxyphenyl group, on the other hand, would probably hinder insertion of **4h** into the relatively smaller BChE acyl-binding pocket, which is a major region of BChE–ligand interaction for multi-ring aromatic compounds [44]. The modest selectivity of compounds **4c**, **4e**, **4g** and **4h** against AChE and BChE in our view make them potential dual inhibitors of both enzymes. Dual inhibition of AChE and BChE, on the other hand, is effective in relieving AD's symptoms with reduced or no side effects [11]. The presence of a lactone moiety in the case of these annulated benzopyran-2-ones and increased conjugation due to the presence of the lipophilic 3,5-dimethoxystyryl arm probably facilitate non-covalent interactions with protein residues and, in turn, promote the inhibition of cholinesterases. The analogous 2-carbo substituted 5-oxo-5*H*-furo[3,2-*g*]chromene-6-

carbaldehydes were previously found to exhibit significantly reduced anticholinesterase activity *in vitro* compared to the reference standards [14].

One of the important therapeutic approaches of AD is the inhibition of β-site amyloid precursor protein (APP) cleaving enzyme-1 (β-secretase or BACE-1), which is involved in the rate-limiting step of the cleavage process of APP leading to the generation of the neurotoxic Aβ protein after the γ-secretase completes its function [45]. The formation and accumulation of fibrillar Aβ peptides in the brain start many years before the first symptoms of AD occur [45], and it is envisaged that inhibition of β-secretase would prevent Aβ formation at an early stage of APP processing, in turn, prevent Aβ neurotoxicity. With the ultimate goal to discover compounds that could inhibit multiple pathological targets related to AD, we evaluated compounds **3** and **4a**–**h** for inhibitory potential against β-secretase activity. Reduced inhibitory activity against β-secretase was observed for **3** ($IC_{50}$ = 23.9 μM) compared to the reference standard, quercetin ($IC_{50}$ = 11.5 μM). The presence of a phenyl ring on position-8 of the furocoumarin-stilbene scaffold resulted in significant activity for **4a** with an $IC_{50}$ value of 18.4 μM. The 8-(3-halogenophenyl) substituted derivatives **4b** ($IC_{50}$ = 27.8 μM) and **4d** ($IC_{50}$ = 30.3 μM) were less inhibiting against this enzyme compared to the isomeric 8-(4-halogenophenyl) substituted derivatives **4c** ($IC_{50}$ = 9.9 μM) and **4e** ($IC_{50}$ = 9.6 μM), respectively. Compounds **4c**, and **4e** not only displayed better dual inhibitory activity against cholinesterase enzymes, but also against β-secretase with lower $IC_{50}$ values than quercetin. Moderate inhibitory activity against β-secretase was also observed for **4f** ($IC_{50}$ = 22.8 μM) substituted with a less polar and non-lipophilic 4-methylphenyl group at the 8-position of the furocoumarin-stilbene scaffold. The 8-(4-methoxyphenyl) **4g** and 8-(3,5-dimethoxyphenyl derivative **4h**, on the other hand, exhibited significant inhibitory effect against β-secretase with $IC_{50}$ values of 17.2 μM and 15.3 μM, respectively. The observed increased inhibitory effect of **4a**–**h** against cholineterases and β-

secretase can be attributed to a combination of the lactone moiety and the planar conjugated aromatic scaffolds.

**Table 1.** AChE, BChE and β-secretase inhibitory activities of compounds **3** and **4a**–**h**.

| Compound | $IC_{50}$ Values in μM | | |
|---|---|---|---|
| | **AChE** | **BChE** | **β-Secretase** |
| **3** | 12.3 ± 0.01 | 9.6 ± 0.02 | 23.9 ± 0.01 |
| **4a** | 10.7 ± 0.02 | 8.3 ± 0.01 | 18.4 ± 0.01 |
| **4b** | 11.6 ± 0.01 | 9.1 ± 0.01 | 27.8 ± 0.02 |
| **4c** | 1.8 ± 0.03 | 3.5 ± 0.02 | 9.9 ± 0.03 |
| **4d** | 21.6 ± 0.04 | 17.6 ± 0.05 | 30.3 ± 0.03 |
| **4e** | 1.9 ± 0.03 | 5.3 ± 0.04 | 9.6 ± 0.01 |
| **4f** | 7.5 ± 0.01 | 13.8 ± 0.03 | 22.8 ± 0.01 |
| **4g** | 3.2 ± 0.01 | 4.5 ± 0.03 | 17.2 ± 0.03 |
| **4h** | 2.8 ± 0.02 | 6.3 ± 0.02 | 15.3 ± 0.02 |
| Donepezil | 0.004 ± 0.02 | 3.13 ± 0.02 | - |
| Galantamine | 1.17 ± 0.02 | 2.05 ± 0.02 | - |
| Quercetin | - | - | 11.5 ± 0.01 |

$IC_{50}$ values (μM) were calculated from log dose inhibition curves, and are expressed as means ± standard deviation (SD) of three independent experiments.

Neuroinflammation is also implicated in the early stages of AD, and studies on animal models previously showed that either LOX-5- or LOX-15 inhibitors have the capability of reducing amyloid and tau pathology as well as improving cognitive impairment [11,46]. Coumarin and related derivatives have been found to intercept arachidonic acid metabolism through LOX or COX inhibition [47]. With drug discovery in AD gradually moving from the

development of molecules with one target, one-disease to the MTDLs capable to address several key pathophysiological processes simultaneously, the scope of the present investigation was also extended to include inhibition of COX-2 and LOX-5 by compounds **3** and **4a**–**h**.

3.2.2. *In Vitro* Inhibitory Assays against COX-2 and LOX-5 and Antioxidant Activity

Compound **3** and its polycyclic derivatives **4a**–**h** were, in turn, evaluated for inhibitory properties through *in vitro* enzymatic assays against the human COX-2 and LOX-5 activities using celecoxib and zileuton as reference standards, respectively. Inhibitory assay against COX-2 revealed that compound **3** and its polycyclic derivatives **4a**–**h** are less active than celecoxib ($IC_{50}$ = 0.007 μM). However, the 8-(3-fluorophenyl) **4b** and 8-(3,5-dimethoxyphenyl) **4h** substituted derivatives were found to be the most active against COX-2 with $IC_{50}$ values of 9.7 μM and 8.6 μM, respectively. LOX-5, an enzyme which modulates Aβ formation is widely distributed within the CNS. Genetic absence of LOX-5 or its pharmacologic inhibition resulted in a significant reduction in brain Aβ levels and deposition in a transgenic AD mouse model suggesting that this enzymatic pathway plays a functional role in modulating the amyloidotic phenotype of this model [48]. Inhibitory assays against LOX-5 activity revealed that compound **3** and its derivatives **4a**–**h** exhibit moderate to significant activity compared to zileuton ($IC_{50}$ = 10.1 μM). The corresponding $IC_{50}$ value for compound **3** is 23.6 μM, while the values for **4a**–**h** range from 13.9 μM to 27.1 μM. Compounds **4b**, **4e** and **4h** substituted with 3-fluorophenyl, 4-chlorophenyl and 3,5-dimethoxyphenyl group on position-8 of the furocoumarin-stilbene scaffold were found to be the most active against LOX-5 with $IC_{50}$ values of 16.3 μM, 15.6 μM and 13.9 μM, respectively. Reduced inhibitory activity against COX-2 and LOX-5 was observed for **4c**, which has been found to exhibit significant inhibitory effect against cholinesterases and β-secretase activity. The analogous 2-carbo substituted 5-oxo-5*H*-furo[3,2-*g*]chromene-6-carbaldehydes were previously found to exhibit reduced inhibitory properties against COX-2 and LOX-5 [14].

Free radicals are important mediators that could aggravate inflammatory processes and their neutralization by radical scavengers and antioxidants is envisioned to reduce inflammation [49]. The antioxidant activity of compounds **3** and **4a**–**h** was first evaluated *in vitro* through the DPPH radical scavenging assay using ascorbic acid as a reference standard (Table 2). Despite reduced inhibitory effect against cholinesterases and β-secretase, compound **4b** was found to exhibit significant activity against COX-2 and LOX-5, and also significant free radical scavenging properties with an $IC_{50}$ value of 10.8 μM compared to ascorbic acid ($IC_{50}$ = 4.2 μM). Compounds **4c**, **4e**, **4g** and **4h**, on the other hand, exhibited moderate to significant antioxidant activities with $IC_{50}$ values of 17.9, 12.5, 18.6 and 6.8 μM, respectively. Compound **4h** substituted with electron-rich methoxy group at the 3- and 5-positions of the phenyl rings of the stilbene arm and the furocoumarin scaffold not only exhibited significant anticholinesterase activity and β-secretase inhibitory activity, but was also found to be the most active molecular hybrid against COX-2 and LOX-5, and also in the DPPH radical scavenging assay.

**Table 2.** Inhibition of COX-2 and LOX-5, and antioxidant activity of **3** and **4a**–**h**.

| | **$IC_{50}$ Values in μM** | | |
|---|---|---|---|
| **Compound** | **COX-2** | **LOX-5** | **DPPH** |
| **3** | 13.2 ± 0.01 | 23.6 ± 0.02 | 15.3 ± 0.03 |
| **4a** | 21.6 ± 0.03 | 19.8 ± 0.02 | 29.7 ± 0.03 |
| **4b** | 9.7 ± 0.03 | 16.3 ± 0.01 | 10.8 ± 0.01 |
| **4c** | 19.5 ± 0.05 | 25.4 ± 0.03 | 17.9 ± 0.02 |
| **4d** | 20.9 ± 0.02 | 18.3 ± 0.02 | 25.7 ± 0.01 |
| **4e** | 12.6 ± 0.01 | 15.6 ± 0.04 | 12.5 ± 0.02 |
| **4f** | 14.8 ± 0.03 | 27.1 ± 0.02 | 8.9 ± 0.03 |
| **4g** | 18.9 ± 0.04 | 22.6 ± 0.01 | 18.6 ± 0.03 |
| **4h** | 8.6 ± 0.02 | 13.9 ± 0.02 | 6.8 ± 0.02 |

| | | | |
|---|---|---|---|
| Celecoxib | 0.007 ± 0.01 | - | - |
| Zileuton | - | 10.1 ± 0.02 | - |
| Ascorbic acid | - | - | 4.2 ± 0.03 |

$IC_{50}$ values (μM) were calculated from log dose inhibition curves, and are expressed as means ± SD of duplicate experiments.

The overproduction of harmful radicals, in particular the ROS results in severe oxidative stress conditions in neurons affected by AD [50]. Since the DPPH radical scavenging assay does not reflect cellular physiological conditions, an *in vitro* cell-based antioxidant activity assay on compounds **4c** and **4h** involving lipopolysaccharide (LPS) induced oxidative stress in the MCF-7 and Hek293 cells was conducted. The $IC_{50}$ values of **4c** and **4h** against the breast MCF-7 cancer cell line obtained through the 3-(4,5-dimethylthiazol-2-yl)-2,5-diphenyltetrazolium bromide (MTT) colorimetric assay using doxorubicin as a reference standard ($IC_{50}$ = 0.8 ± 0.07 μM) were found to be 2.1 ± 0.38 μM, 1.4 ± 0.23 μM, respectively. The $IC_{50}$ values for **4c**, **4h** and doxorubicin, against the Hek293-T cells, on the other hand, were found to be 3.2 ± 0.51 μM, 5.4 ± 0.62 μM and 1.2 ± 0.45 μM, respectively. Both MCF-7 and Hek-293-T cells showed increased sensitivity to doxorubicin in analogy with the literature precedent [51]. Compounds **4c** and **4h**, also exhibited significant cytotoxicity against the MCF-7 cancer cell line and the normal cells. Based on the cytotoxicity results, one concentration less than the $IC_{50}$ (1 μM) that does not kill the cells was selected to investigate the compounds suppression effects of LPS-induced ROS production. Data was processed and analysed using ANOVA followed by the Duncan's multiple comparison test. When LPS was added to the MCF-7 and Hek293-T cells, respectively, the amount of ROS produced increased dramatically. Compounds **4c** and **4h** in the presence of LPS, on the other hand, supressed 66% and 68% of ROS in cancer MCF-7 cells, respectively (Figure 2a). Moderate ROS reduction (about 45%) was observed for **4h**, while **4c** showed significant

ROS reduction in normal Hek293-T cells (Figure 3b). Literature precedent revealed that ROS levels are elevated in many human cancer cells compared to those in their normal counterparts [52].

**(a)**

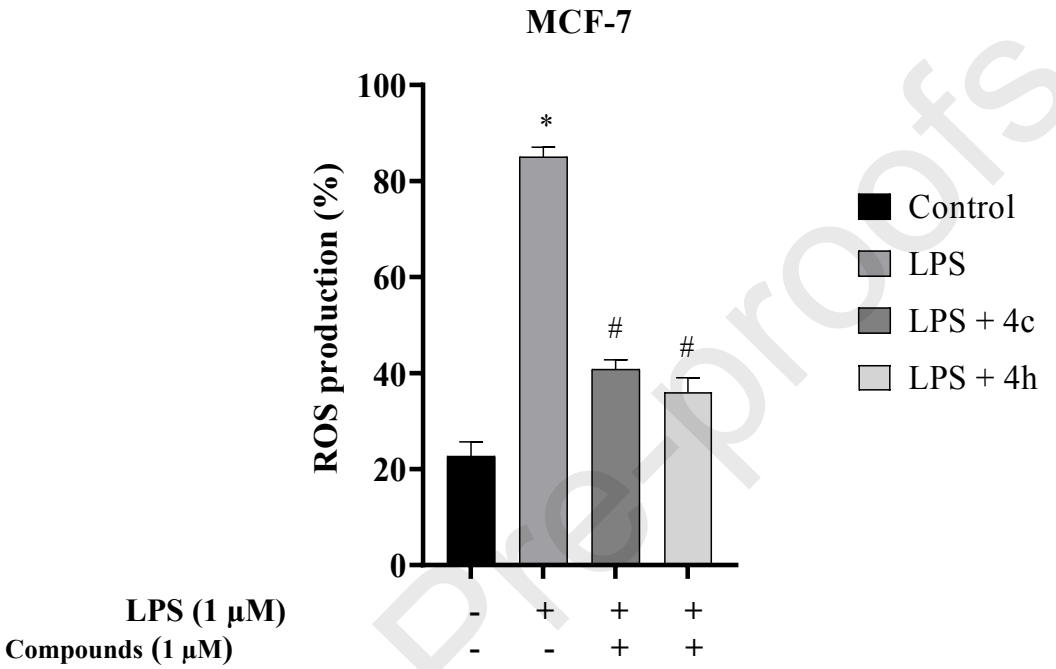


**(b)**

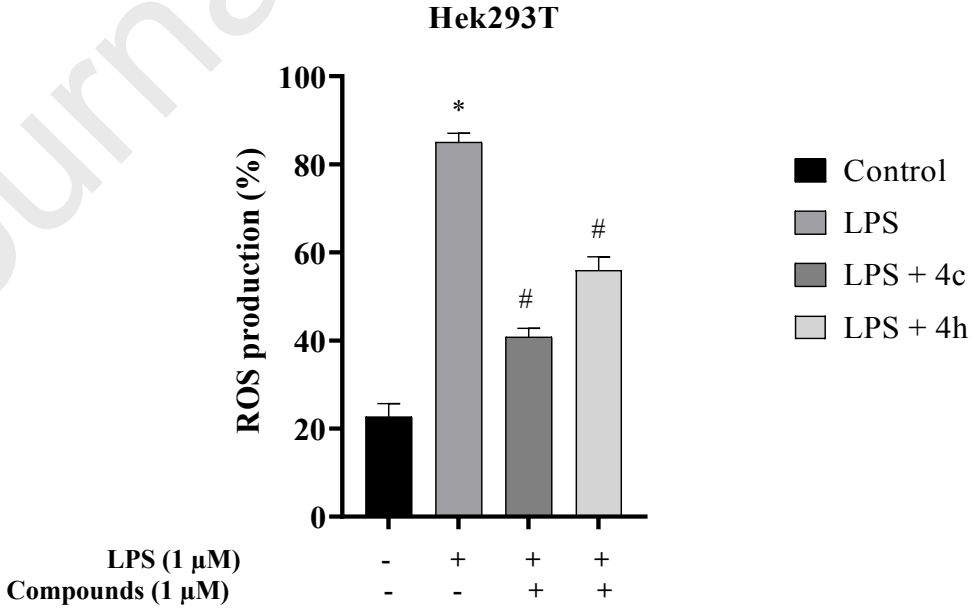

**Figure 2:** Effects of compounds **4c** (a) and **4h** (b) on LPS-induced ROS production in MCF-7 (a) and HEK293 cells (b). Data is expressed as mean ± SD (n = 3). Symbols * and # indicate a significant difference from untreated and treated cells.

Compound **4c**, which exhibited the most potent cholinesterase (AChE and BChE) and β-secretase inhibitory activity in the series, and derivative **4h** found to be more active against COX-2 and LOX-5 were selected for kinetic analyses to establish their modes of inhibition.

3.3. Kinetic studies of **4c** and **4h** on AChE and BChE and β-secretase

The mechanisms of action of compounds **4c** and **4h** against these key enzyme targets associated with AD were evaluated by constructing the Lineweaver-Burk double reciprocal plots and the Dixon plots at increasing inhibitor and substrate concentrations. The corresponding graphs for these compounds against AChE, BChE and β-secretase have been included as Figures S2, Figures S3 and Figures S4 in the Supplementary Information (SI). The Lineweaver-Burk plot of **4c** against AChE (Figure S2.1a) shows a decrease in the $V_{max}$ values (0.037–0.018) with an increase in the Michaelis constant ($K_m$) values (0.13–0.19). Sets of straight lines intersect above the x-axis for both the Lineweaver-Burk plot and the Dixon plot (Figure S2.1b) with a $K_i$ value of 1.30 ± 0.05 μM. The observed results suggest a mixed mode of inhibition for **4c**, which probably binds to PAS and CAS residues of AChE. Compound **4h** on AChE (Figure S2.2a), on the other hand, shows a decrease in $V_{max}$ values (0.054–0.017) with relatively unchanged $K_m$ value of 0.22. The Dixon plot of **4h** (Figure S2.2b) shows set of straight lines intersecting on the x-axis with $K_i$ value of 1.31 ± 0.01 μM. Kinetic data, for **4h** suggest a non-competitive mode of inhibition for this compound. The Lineweaver-Burk plot of compound **4c** against BChE (Figure S3.1a) shows a decrease in the $V_{max}$ values (0.096–0.021) and a constant $K_m$ value of 0.23, indicative of non-competitive inhibition. The set of straight lines for the Dixon plot (Figure S3.1b) for this compound, intersect on the x-axis with $K_i$ value of 3.2 ± 0.04 μM, which also suggest a non-competitive mode of action. There is a decrease in the $V_{max}$ values (0.041–0.021)

of **4h** and the $K_m$ values are less affected with the set of straight lines intersecting above the x-axis. The straight lines also intersect above the x-axis of the Dixon plot with a Ki value of 1.89 ± 0.05 μM, which is indicative of competitive mode of inhibition. The enzyme kinetic of compounds **4c** and **4h** against BACE-1 was also undertaken. The Lineweaver-Burk plot of **4c** (Figure S4.1a) at increasing inhibitor concentration (0–16 μM) shows a decrease in both $K_m$ (0.0023–0.0012) and $V_{max}$ (0.007–0.003) values. The set of straight lines for both the Lineweaver-Burk and Dixon plots intersect above the x-axis confirming a mixed mode of inhibition. The $K_i$ for compound **4c** determined from the Dixon plot (Figure S4.1b) is 1.28 ± 0.04 μM. The Lineweaver-Burk plot of **4h** (Figure S4.2a) shows a decrease in $V_{max}$ values (0.016–0.004) with a relatively unchanged Michaelis constant ($K_m$) value (0.035). The set of straight lines intersect on the x-axis of the Dixon plot (Figure 4.2b) with $K_i$ value 4.80 ± 0.03 μM, typical of a non-competitive mode of action. In an effort to understand the plausible drug-receptor interactions on a molecular level, molecular docking (*in silico*) was used to predict the hypothetical binding orientation and interaction of these compounds in the active pockets of these enzymes.

3.4. Molecular Docking Studies into AChE, BChE, BACE-1, COX-2 and LOX-5 Active Sites

The test compounds and the reference standard were docked within the binding sites of AChE, BChE, β-secretase, COX-2 and LOX-5. Compound **4c** which is the highest inhibiting compound within the series against cholinesterases (AChE and BChE) and exhibited significant activity against β-secretase, and **4h** with the highest activity against LOX-5 and COX-2 were selected as representative examples to elucidate the protein-ligand interactions of the test compounds, which could be useful for future ligand optimization or design. To better explain the activity of compounds **4c** and **4h** in relation with the interactions between the ligand and the potential target, the least active **4d** was also docked against the targets assayed in this study.

Moreover, the pharmacokinetic properties of compounds **4c** and **4h** have also been calculated and the corresponding results also discussed below.

3.4.1. Docking of the test compounds into AChE, BChE and β-Secretase Active Sites

The test compounds were docked within the binding sites of AChE (PDB: 6O4W), BChE (PDB: 4BDS) and β-secretase (PDB: 6UVP) and their docking poses are included as Figures S3a, S3b and S3c in SI, respectively. The control dockings of AChE, BChE and β-secretase have the root mean square deviation (RMSD) values of 0.56 Å, 0.58 Å and 0.67 Å, respectively, showing the appropriateness of the used parameters. The calculated binding free energy of the test compounds are represented in Table S1 (refer to SI). The affinity of compound **3** is predicted to be relatively lower than that of donepezil against AChE and BChE. Although less active than donepezil, the calculated free binding energy values for the test compounds against AChE approach that of this reference standard, while those for BChE are better than donepezil. The test compounds also showed more favourable binding affinity for β-secretase when compared to the reference standard, quercetin. Literature precedent revealed that the binding energies obtained through molecular docking do not always correlate well with the biological response observed in the *in vitro* tests [53]. Nevertheless, the hypothetical binding orientation and interaction of small molecules and drug candidates with protein targets are useful in rationalizing structure activity relationship and for future ligand optimization. The active site of AChE is a 20 Å deep gorge divided into two sub-sites: the peripheral anionic site (PAS) located at the entrance of the gorge composed of five protein residues (Tyr72, Asp74, Tyr124, Trp286 and Tyr341) and the catalytic anionic site (CAS) located close to the bottom of the gorge CAS is composed of the catalytic triad (Ser203, His447, Glu334), an oxyanion hole (Gly121, Gly122, Ala204), an acyl-binding pocket (Trp233, Phe288, Phe290, Phe292, Phe330, Phe331) and a choline binding site (Trp86, Tyr337, Phe338) [54]. Donepezil is known to interact with both CAS and PAS tryptophans of AChE via ring-stacking interactions [55]. Ring-ring stacking interactions are predicted between

donepezil and the residues Trp86 and Trp286 (Figure 3a). The planar aromatic coumarin scaffold is lipophilic, and able to interact with lipophilic binding sites by establishing strong hydrophobic and aromatic–aromatic stacking interactions with aromatic amino acids such as Phe, Tyr, and Trp [56]. Molecular docking study of **4c** (Figure 3a) shows ring-ring (π–π stacking and π–π T-shaped) interactions with crucial amino acids present at the catalytic active site (CAS), mid-gorge and PAS of AChE. The furocoumarin scaffold of this compound is docked at AChE PAS Tyr341 region and there is hydrogen bonding interaction between its carbonyl oxygen and the protein residue Arg296. The fluorobenzene ring is surrounded by the protein residues Tyr72 (π–π interaction), Asp74 (electrostatic interaction) and Trp286 (π–π T-shaped interaction) at the entrance of the gorge. This orientation may provide additional beneficial effect due to interaction of the halogen atom with aromatic residues, specifically Tyr72 phenol side chain, in active site of AChE [57]. No such interaction is predicted for compound **4d** against AChE, and this compound has one π-π ring interaction less than **4c** (Figure S4a in SI). The carbon-carbon double bond bridge enabled the 3,5-dimethoxyphenyl group of the stilbene moiety to extend into the CAS region of AChE to be flanked by Ser203 of the catalytic triad, Gly121 in the oxyanion hole and the residues Tyr337 and Phe338 of the choline binding site. The predicted strong interactions of **4c** with protein residues in PAS and CAS of AChE are consistent with the observed mixed kinetic type of inhibition for this compound. Compounds with capability for binding simultaneously to PAS and CAS sites of AChE not only improve cognition by inhibiting AChE, but also prevent the pro-aggregating activity of AChE toward β-amyloid (Aβ) [58].

Figure 3b shows the docking poses of donepezil and **4c** in the active pocket of BChE with calculated binding energies of -8.56 kcal/mol and -8.79 kcal/mol, respectively. There is π-π ring interactions between donepezil and Trp82 of BChE. Compound **4c** is predicted to be involved in π-π ring interactions with the protein residues Trp82 and Trp231. The styryl moiety of this compound extends towards the region of serine (Ser198) and histidine (His438) of the catalytic

triad, which may account for the increased inhibitory effect of this compound against BChE. This compound might also bind additional alternative sites on the enzyme consistent with its non-competitive inhibition mode. Compound **4d**, on the other hand, is predicted to exhibit slightly less π-π interactions (four interactions) and hydrophobic contacts (14 contacts) compared to **4c** (five π-π interactions and 17 hydrophobic contacts) (Figure S4b in SI).

The docking poses of quercetin and compound **4c** into β-secretase are represented in Figure 3c. Compound **4c** showed more favourable binding affinity for β-secretase compared to the reference standard, quercetin, with calculated binding energy values of -6.97 kcal/mol and -6.49 kcal/mol, respectively. Docking pose of **4c** into this enzyme's active site revealed that it is stabilized by two hydrogen bonding interaction between the methoxy group of the styryl moiety and Thr72 of the S1′ pocket, two parallel-displaced π-π interactions with Tyr71 and Phe108, and also two T-shaped π-π interactions (Trp115 and Phe109) at the furocoumarin region. The ring stacking observations are similar with the findings by Haghighijoo *et al*. 2017 whereby Tyr71 of S1 sub-pocket was noticed to be the main regulator for the open and closed conformation of BACE-1 [59]. In addition, Asp228 (pKa 3.41) of BACE-1 catalytic site could be protonated during the inhibition assay as previously observed by Huang *et al.* [60]. This probably accounts for the key hydrogen bonding interaction of this residue with the methoxy group of the styryl arm of **4c**. Increased interactions of this compound with the protein residues in the active site of β-secretase may account for this compound's increased inhibitory effect against this enzyme activity. Although compound **4d** is predicted to have one extra π-π interaction and one hydrophobic contact with BACE-1 (Figure S4c in SI) compared to **4c**, no hydrogen bonding interaction is predicted between the former compound and the receptor. These simulated results are consistent with the observed inhibitory effects of these compounds with $IC_{50}$ values 9.9 ± 0.03 μM (**4c**) and 30.3 ± 0.03 μM (**4d**), and their calculated binding affinities -6.97 kcal/mol and -6.86 kcal/mol, respectively.

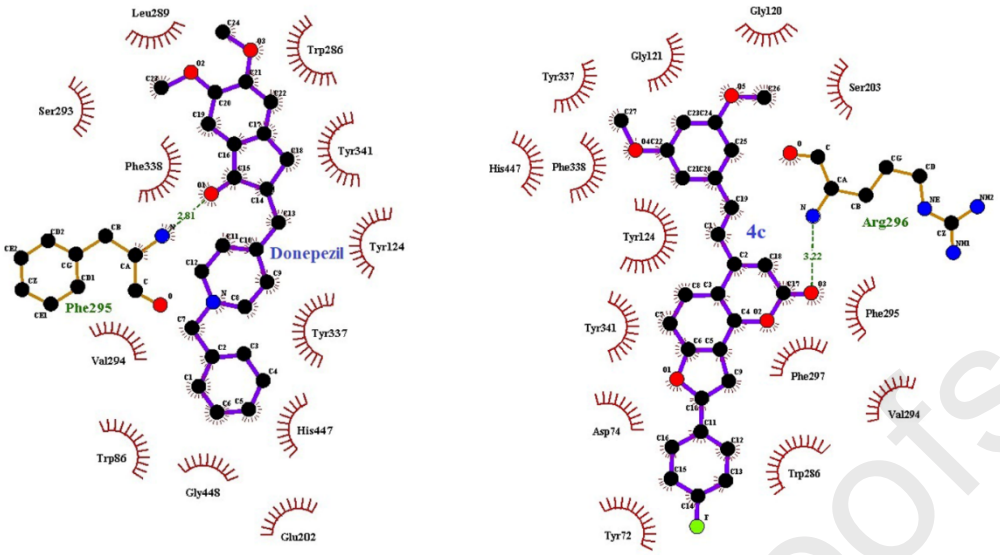


(a)

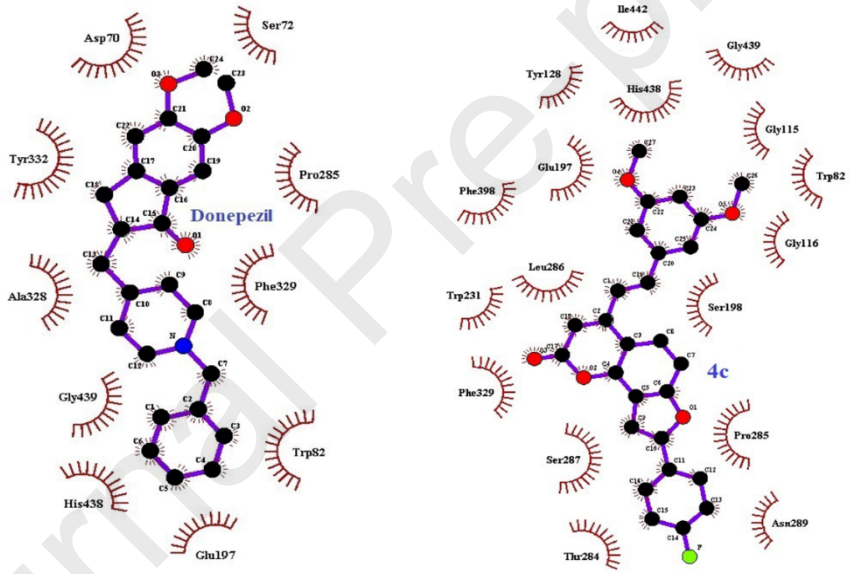


(b)

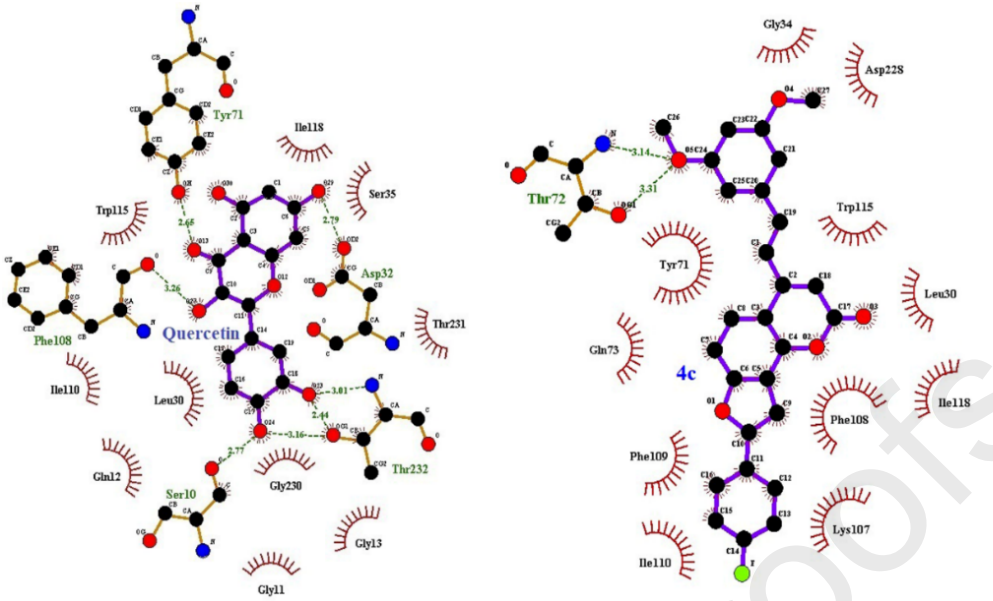


(c)

**Figure 3:** The interactions of donepezil/quercetin and compound **4c** in the active site of AChE (3a), BChE (3b) and β-secretase (3c).

3.4.2. Docking of **4h** to COX-2 (PDB: 5IRK), COX-1 (PDB: 4O1Z) and LOX-5 (PDB: 3O8Y).

The docking poses of celecoxib and compound **4h** into COX-2 are represented in Figure 4a and their corresponding calculated binding energy values (Table S2 in SI) are -10.72 kcal/mol and -10.41 kcal/mol, respectively. Celecoxib is stabilized by ten hydrophobic contacts, three π-π interactions and four hydrogen bonding interactions with COX-2, which are responsible for the increased inhibitory effect of this drug against this inducible isoform. The dimethoxyphenyl ring of the stilbene arm of **4h** is involved in π-π stacking interaction with Tyr355 while the protein residues Tyr348, Tyr385, Tyr387 and Phe518 are involved in similar interactions with the dimethoxyphenyl ring on the furan moiety. However, no hydrogen bonding interaction is predicted between this compound and COX-2. The high number of hydrophobic contacts (19 contacts) predicted for compound **4h** with COX-2 has presumably contributed to the favourable binding and significant inhibitory effect against this enzyme. Seventeen hydrophobic contacts are predicted between compound **4d** (-9.78 kcal/mol) and the protein residues of COX-2 (Figure S6a in SI). The substitution of long-side-chain amino acids Ile523, His513 and Ile434 in

cyclooxygenase-1 (COX-1) with Val523, Arg513 and Val434 in COX-2 resulted in the enlargement of the hydrophobic substrate-binding channel and the formation of the additional hydrophilic side pocket in the cyclooxygenase active site of COX-2 [61]. In an attempt to rationalize the selectivity of **4h** towards COX-2 over COX-1 at least at theoretical level, we docked celecoxib and compound **4h** into COX-1 (Figure 4b). Celecoxib (-8.79 kcal/mol) is stabilized by 12 hydrophobic contacts, two π-π interactions and two hydrogen bonding interactions with COX-1. Molecular docking predicts 19 hydrophobic interactions between **4h** (-10.52 kcal/mol) and the protein residues in the active site with no hydrogen bonding interaction. The docking pose of **4d** into COX-1 active site (Figure S6b in SI), on the other hand, shows 18 hydrophobic contacts and one hydrogen bonding interaction. This compound is predicted to have comparable affinity for both cyclooxygenases (COX-1 and COX-2) with calculated binding energy value of -9.78 kcal/mol. The predicted results in the case of **4h** can be attributable to the topological features and general size of the binding site of COX-1, which is smaller than that of COX-2. As a result, larger and more hydrophilic compounds easily fit into the large catalytic site of this inducible isoform of COX, thus increasing its spectrum of possible inhibitors. Increased hydrophobic interactions of **4h** with respect to amino acid residues in COX-2 can be supportive evidence in developing this compound as a selective COX-2 inhibitor.

Evaluation of compounds **4d** and **4h** against LOX-5 resulted in higher binding affinity -6.45 kcal/mol and -6.76 kcal/mol, respectively, compared to zileuton (-4.61 kcal/mol). Although zileuton is docked at similar binding site with **4d** or **4h** it is oriented in a perpendicular direction (Figure S5c, SI). The docking pose of zileuton shows six hydrophobic contacts with LOX-5 and the amide end of this ligand is making three hydrogen bonds by facing Lys173 and Glu412 (Figure 4c). Compound **4h** docked at the shallow surface of LOX-5 presumably because of the inaccessible binding cavity of this enzyme by the test compounds. Earlier study suggested that in order to access the binding site of LOX-5, the cavity needs to undergo conformational changes

[62]. Figure 4c also shows that both the dimethoxyphenyl ends of compound **4h** are involved in hydrogen bonding interactions with LOX-5, consistent with the most favourable calculated binding affinity and the observed increased inhibitory effect of this compound against this enzyme. Figure S6c in SI shows the docking pose of compound **4d** (-6.45 kcal/mol) in the binding pocket of LOX-5 (Figure S6c in SI), and this compound is predicted to exhibit similar interactions with **4h** (-6.76 kcal/mol). Their calculated binding energy values are consistent with the observed inhibitory activity of these compounds against LOX-5 with $IC_{50}$ values 18.3 ± 0.02 µM and 13.9 ± 0.02 µM, respectively.

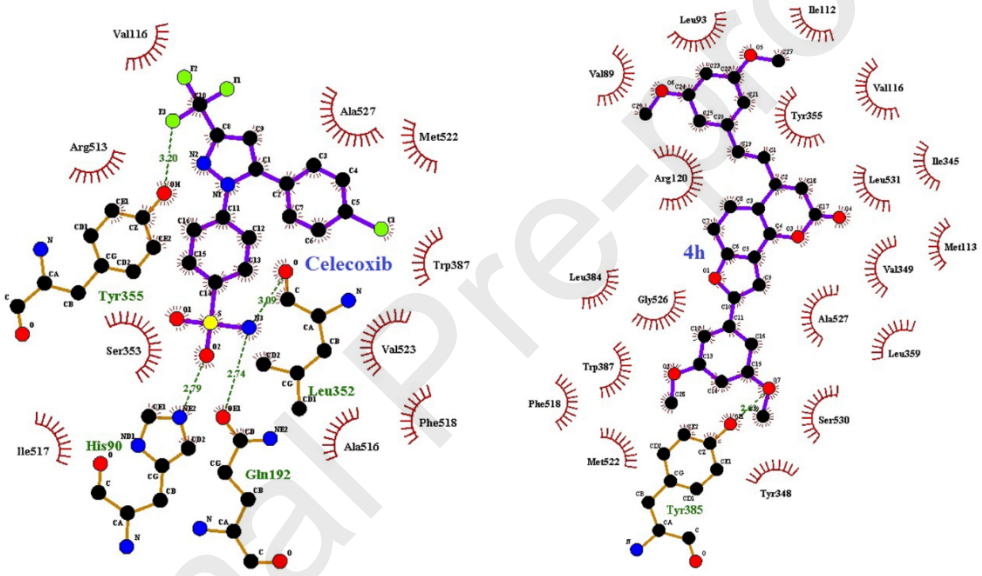


(a)

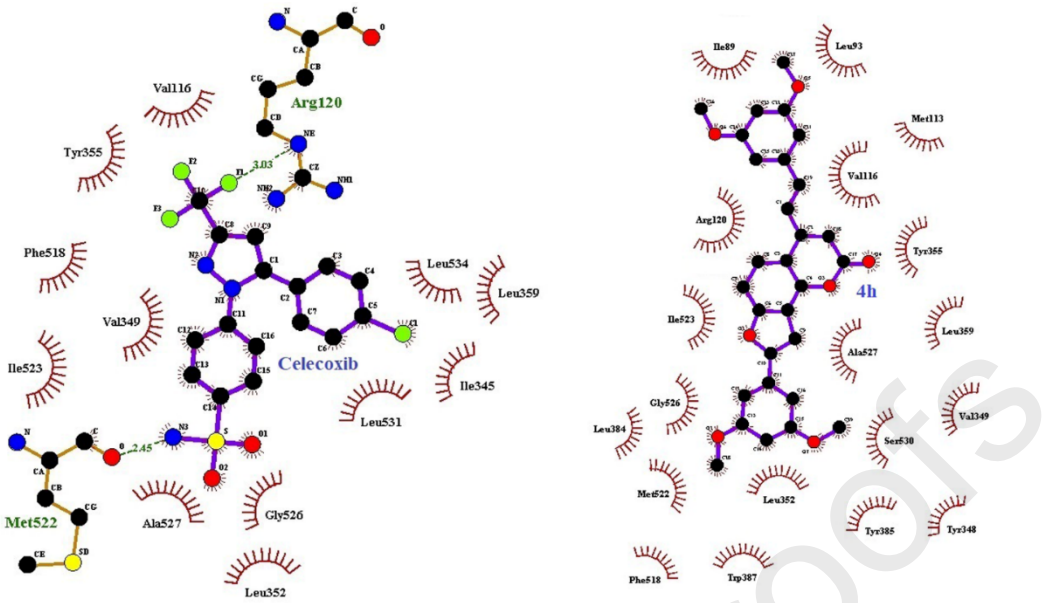


(b)

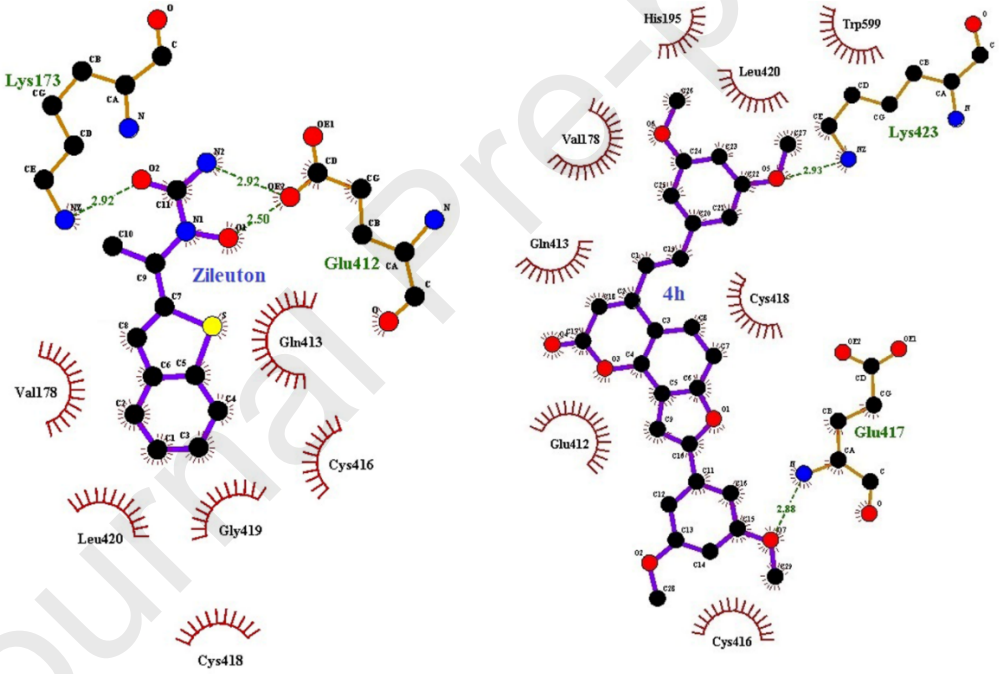


(c)

**Figure 4:** The interactions of celecoxib, zileuton and compound **4h** in the active site of COX-2 (4a), COX-1 (4b) and LOX-5 (4c).

3.4.3. Pharmacokinetics properties prediction of compounds **4c** and **4h**

The drug likeness of compounds **4c** (highest inhibiting compound against AChE, BChE and β-secretase) and **4h** (highest activity against LOX-5 and COX-2) was estimated by calculating

molecular descriptors using Molinspiration tool and the corresponding results are presented in Table 3. The pharmacokinetics prediction data showed that compounds **4c** and **4h** would exhibit absorption percentage > 80%, suggesting the possible development as oral drug candidates. In addition, the calculated data did not violate more than one of the Lipinski's rule of five (octanol-water partition coefficient logP ≤ 5, molecular weight ≤ 500, number of hydrogen bond acceptors ≤ 10 and number of hydrogen bond donors ≤ 5), thus further showing the drug-like properties of compounds **4c** and **4h**. The latter has more rotatable bonds (7) indicating more flexibility than **4c** with 5 rotatable bonds. The BBB predictions also showed the positive permeability of compounds **4c** and **4h** in passing the BBB. Compound **4h** would probably have the efficacy on the brain-specific targets.

**Table 3.** Pharmacokinetics properties predictions of compounds **4c** and **4h**.

| | **Compound** | |
|---|---|---|
| **Property** | **4c** | **4h** |
| miLogP | 6.72 | 6.60 |
| Topological polar surface area (Å) | 61.82 | 80.29 |
| Absorption (%) | 87.67 | 81.30 |
| Number of atom | 33 | 36 |
| Molecular weight | 442.44 | 484.50 |
| Molecular volume | 380.40 | 426.56 |
| Hydrogen bond acceptor | 5 | 7 |
| Hydrogen bond donor | 0 | 0 |
| Rotatable bonds | 5 | 7 |
| Lipinski's violation | 1 | 1 |
| Blood-brain barrier (BBB) | + | + |

miLogP: logarithm of partition coefficient of compound between *n*-octanol and water; ABS percentage = 109 - (0.345 x Topological polar surface area) [63].

## 4. Conclusions

Our *in vitro* and *in silico* investigations established the enzyme inhibitory effects of the 4-stilbene appended furocoumarin hybrids on AChE, BChE, β-secretase, COX-2 and LOX-5; all of which are related to mechanisms that underpin Alzheimer's disease. An extended conjugation resulted in increased inhibitory effect against both AChE and BChE as well as β-secretase. This observation is attributed to a combination of the furobenzopyran-2-one nucleus and the lipophilic 3,5-dimethoxystyryl wing, which have previously been found to increase cholinesterase activity. Derivatives **4c** and **4e** with halogen atom on the *para* position of the 7-phenyl ring or **4g** and **4h** with methoxy substituent/s on the 7-phenyl generally exhibited increased activity against several of the biochemical targets assayed including antioxidant effect. Compounds **4c**, **4e**, **4g** and **4h** were found to exhibit dual cholinesterase and β-secretase inhibitory effect as well as free radical scavenging activity. The kinetic study revealed that the most active compound **4c** against the human AChE is a mix-type inhibitor, which binds to PAS and CAS of AChE. This observation is consistent with molecular modelling studies, which suggested that this furocoumarin-stilbene hybrid interacts with residues in the PAS and CAS regions of AChE. AChE inhibitors that interact with both CAS and PAS sites simultaneously can interfere with the aggregation of Aβ protein while enhancing the inhibitory activity of AChE, and play a dual role in the treatment of AD. Compound **4h** has also been found to exhibit anti-inflammatory and cytotoxic properties besides other effects like anticholinesterase, β-secretase and antioxidant activities, consistent with the design idea. The results of this study stress the importance of the benzopyran-2-one and conjugative effect of the surrounding substituents on biological activity of the furochromenone

analogues. Taken together, these preliminary findings highlight this class of compounds particularly of **4c** and **4h** as potential multi-functional anti-Alzheimer's agents deserving further studies aimed at improving the physicochemical properties for drug bioavailability (eg., aqueous solubility) including their safety profile. One of the basic features of anti-AD drugs is their ability to reach therapeutic targets in the CNS, and it will also be important to evaluate this parameter in the development of these molecular hybrids as anti-AD agents.

**Supplementary Materials:** Table S1 and S2: The estimated binding free energy of the test compounds with AChE, BChE and β-secretase from molecular docking simulation, and with COX-2 and LOX-5 from molecular docking simulation, respectively, Figure S1: $^{1}$H-NMR and $^{13}$C-NMR spectra of the prepared compounds, Figure S2: Lineweaver-Burk and Dixon plots of **4c** and **4h** against AChE, BChE and BACE-1, Figure S3: The docked conformation of donepezil, quercetin and the test compounds in the binding pocket of AChE, BChE and BACE-1, Figure S4: The interactions of compound **4d** in the active site of AChE, BChE and β-secretase, Figure S5: The docked conformations of celecoxib, zileuton and the test compounds in the binding pocket of COX-2, COX-1 and LOX-5, and Figure S6: The interactions of **4d** in the active site of COX-2, COX-1 and LOX-5.

**Author contribution:** Conceptualization and writing of the manuscript, M.J.M.; review and editing the paper, M.J.M.; S.G. and YSC; revising, M.J.M., experimentation ENA and GKM (on cytotoxicity).

**Acknowledgments:** This project was funded by the University of South Africa and the National Research Foundation (NRF) in South Africa (NRF GUN: 118554). YSC thanks Universiti Sains Malaysia for RUi grant (1001/CIPPM/8011051). We also thank the University of Stellenbosch Central Analytical Facility (CAF) for mass spectrometric and elemental analyses.

**Conflicts of Interest:** The authors declare no conflict of interest.

**References**

[1] M.W. Bondi, E.C. Edmonds, D.P. Salmon, Alzheimer's disease: Past, Present, and Future. J. Int. Neuropsychol. Soc. 23 (2017) 818–831.

[2] Y. Christen, Oxidative stress and Alzheimer disease. Am. J. Clin. Nutr. 71 (2000) 621S–629S.

[3] Z. Yang, Q. Song, Z. Cao, G. Yu, Z. Liu, Z. Tan, Y. Den, Design, synthesis and evaluation of flurbiprofen-clioquinol hybrids as multitarget-directed ligands against Alzheimer's disease. Bioorg. Med. Chem. 289 (2020) 115374.

[4] N. Kishore, P. Kumar, K. Shanker, A.K. Verma, Human disorders associated with inflammation and the evolving role of natural products to overcome. Eur. J. Med. Chem. 179 *(*2019) 272–309.

[5] L.J. Van Eldik, M.C. Carrillo, P.E. Cole, D. Feuerbach, B.D. Greenberg, J.A. Hendrix, M. Kennedy, N. Kozauer, R.A. Margolin, J.L. Molinuevo, R. Mueller, R.M. Ransohoff, D.M. Wilcock, L. Bain, K. Bales, The roles of inflammation and immune mechanisms in Alzheimer's disease. Alzheimer's Dement. 2 (2016) 99–109.

[6] H. Gocer, F. Topal, M. Topal, M. Küçük, D. Teke, I. Gulcin, S.H. Alwasel, C.T. Supuran, Acetylcholinesterase and carbonic anhydrase isoenzymes I and II inhibition profiles of taxifolin. J. Enzym. Inhib. Med. Chem. 31 (2016) 441–447.

[7] V. Hachinski, T.-Y. Lee, Commentary on "Alzheimer's disease drug development and the problem of the blood-brain barrier." The blood-brain barrier: A physical and conceptual challenge**.** Alzheimers Dement. 5 (2009) 435–436.

[8] W.A. Banks, Drug delivery to the brain in Alzheimer's disease: Consideration of the blood-brain barrier. Adv. Drug Deliv. Rev. 64 (2012) 629–639.

[9] M.B. Colovic, D.Z. Krstic, T.D. Lazarevic-Pasti, A.M. Bondzic, V.M. Vasic, Acetylcholinesterase inhibitors: Pharmacology and toxicology. Curr. Neuropharmacol. 11 (2013) 315–335.

[10] M. Bajda, N. Guzior, M. Ignasik, B. Malawska, Multi-target-directed ligands in Alzheimer's disease treatment. Curr. Med. Chem. 18 (2011) 4949–4975.

[11] C.G. Ballard, Advances in the treatment of Alzheimer's disease: Benefits of dual cholinesterase inhibition. Eur. Neurol. 47 (2002) 64–70.

[12] E.D. AlFadly, P.A. Elzahhar, A. Tramarin, S. Elkazaz, H. Shaltout, M.-M. Abu-Serie, J. Janockova, O, Soukup, D.A. Dhareeb, A.L. El-Yazbi, R.W. Rafeh, N.-M.Z. Bakkar, F. Kobeissy, I. Iriepa, I. Moraleda, M.N.S. Saudi, M. bartolini, A.S.F. Belal, Tackling neuroinflammation and cholinergic deficit in Alzheimer's disease: Multi-target inhibitors of cholinesterases, cyclooxygenase- and 15-lipoxygenase. Eur. J. Med. Chem. 167 (2019) 161–186.

[13] A. Ibrar, S.A. Shehzadi, F. Saeed, I. Khan, Developing hybrid molecule therapeutics for diverse enzyme inhibitory action: Active role of coumarin-based leads in drug discovery, Bioorg Med. Chem. 26 (2018) 3731–3762.

[14] M.J. Mphahlele, E.N. Agbo, S. Gildenhuys, I.B. Setshedi, Exploring biological activity of 4-oxo-4*h*-furo[2,3-*h*]chromene derivatives as potential multi-target-directed-ligands inhibiting cholinesterases, β-secretase, cyclooxygenase-2 and lipoxygenase-5/15. Biomolecules 9 (2019) 736–760.

[15] N. Kitamura, S. Kohtani, R. Nakagaki, Molecular aspects of furocoumarin reactions: Photophysics, photochemistry, photobiology, and structural analysis J. Photochem. Photobiol. C: Photochem. Rev. 6 (2005) 168–185.

[16] L.D. Via, O. Gia, S. Caffieri, Gracía-Argáz, A. Quezada, E. Uriarte, A novel tetrahydrobenzoangelicin with dark and photo biological activity. Bioorg. Med. Chem. 20 (2012) 3603–3608.

[17] K.C. Fylaktakidou, D.J. Hadjipavlou-Litina, K.E. Litinas, D.N. Nicolaides, Natural and synthetic coumarin derivatives with anti-inflammatory/antioxidant activities. Curr. Pharm. Design. 10 (2004) 3813–3833.

[18] K.C. Fylaktakidou, D.J. Hadjipavlou-Litina, K.E. Litinas, D.N. Nicolaides, Natural and synthetic coumarin derivatives with anti-inflammatory/antioxidant activities. Curr. Pharm. Design. 10 (2004) 3813–3833.

[19] H. Özbek, Z. Güvenalp, G. Yilmaz, K.O. Yerdelen, C. Kazaz, Ö.L. In vitro anticholinesterase activity and molecular docking studies of coumarin derivatives isolated from roots of *Heptaptera cilicica.* Med. Chem. Res. 27 (2018) 538–545.

[20] S. Marumoto, M. Miyazawa, Biotransformation of isoimperatorin and imperatorin by *Glomerella cingulate* and β-secretase inhibitory activity. Bioorg. Med. Chem. 18 (2010) 455–459.

[21] G. Somani, C. Kulkami, P. Shinde, R. Shelke, K. Laddha, S. Sathaye, *In vitro* acetylcholinesterase inhibition by psoralen using molecular docking and enzymatic studies. J. Pharm. Bioallied Sci. 7 (2015) 32–36.

[22] L.G. de Souza, M.N. Rennó, J.D. Figueroa-Villar, Coumarins as cholinesterase inhibitors: A review. Chem. Biol. Interact. 254 (2016) 11–23.

[23] S. Marumoto, M. Miyazawa, Structure–activity relationships for naturally occurring coumarins as β-secretase inhibitor. Bioorg. Med. Chem. 20 (2012) 784–788.

[24] P. Penalver, E. Belmonte-Reche, M. Adán, M. Caro, M.L. Maeos-Martin, M. Delgado, E. González-Rey, J.C. Morales,. Alkylated resveratrol metabolites as potential therapeutics for neurodegenerative diseases. Eur. J. Med. Chem. 146 (2018) 123–138.

[25] F.B. Belluti, G. Fontana, L. Dal Bo, N. Carenini, C. Giommarelli, F. Zunino, Design, synthesis and anticancer activities of stilbene-coumarin hybrid compounds: Identification of novel proapoptotic agents. Bioorg. Med. Chem. 18 (2010) 3543–3550.

[26] B. De Filippis, A. Ammazzalorso, M. Fantacuzzi, L. Giampietro, C. Maccallini, R. Amoroso, Anticancer activity of stilbene-based derivatives. ChemMedChem 12 (2017) 558–570.

[27] Y.X. Li, X.M. Qiang, Y. Li, X. Yang, L. Luo, G.Y. Xiao, Z.C. Cao, Z.H. Tan, Y. Deng, Pterostilbene-O-acetamidoalkylbenzylamines derivatives as novel dual inhibitors of cholinesterase with anti-β-amyloid aggregation and antioxidant properties for the treatment of Alzheimer's disease. Bioorg. Med. Chem. Lett. 26 (2016) 2035–2039.

[28] J.A. Joseph, D.R. Fisher, V. Cheng, A.M. Rimando, B. Shukitt-Hale, Cellular and behavioral effects of stilbene resveratrol analogues: implications for reducing the deleterious effects of aging. J. Agr. Food Chem. 56 (2008) 10544–10551.

[29] J. Chang, A. Rimando, M. Pallas, A, Camins, D. Porquet, J. Reeves, B. Shukitt-Hale, M.A. Smith, J.A. Joseph, G. Casadesus, Low-dose pterostilbene, but not resveratrol, is a potent neuromodulator in aging and Alzheimer's disease. Neurobiol. Ag. 33 (2012) 2062–2071.

[30] C. Rivière, T. Richard, L. Quentin, S. Krisa, J.M. Mérillon, J.P. Monti, Inhibitory activity of stilbenes on Alzheimer's beta-amyloid fibrils in vitro. Bioorg. Med. Chem. 15 (2007) 1160–1167.

[31] R.A. Herrera, W. Castrillón, E. Otero, E. Ruiz, M. Carda, R. Agut, T. Naranjo, G. Moreno, M.E. Maldonado, G, W. Cardona, Synthesis and antiproliferative activity of 3- and 7-styrylcoumarins. Med. Chem. Res. 27 (2018) 1893–1905.

[32] Y.R. Li, S. Li, C.-C. Lin, Effect of resveratrol and pterostilbene on aging and longevity. BioFactors 1 (2018) 69–82.

[33] F. Arduini, I. Errico, A. Amine, L. Micheli, G. Palleschi, D. Moscone, Enzymatic spectrophotometric method for aflatoxin B detection based on acetylcholinesterase inhibition. Anal. Chem. 79 (2007) 3409–3415.

[34] K. Zhu, H. Zhou, H. Qian, Antioxidant and free radical scavenging activities of wheat germ protein hydrolysates (WGPH) prepared with alcalase. Process Biochem. 41 (2006) 1296–1302.

[35] T. Mosmann, Rapid colorimetric assay for cellular growth and survival: Application to proliferation and cytotoxicity assays. J. Immunol. Methods. 65 (1983) 55–63.

[36] S. Chen, C. Hsu, M. Tsai, R. Chen, Inhibition of oxidative stress by low-molecular-weight polysaccharides with various functional groups in skin fibroblasts. Int. J. Mol. Sc. 14 (2013) 19399–19415.

[37] W.Y. Wu, Y.Y. Wu , H. Huang, C. He, W.Z. Li, H.L. Wang, H.-Q. Chen, Y.-Y. Yin Biochanin A attenuates LPS-induced pro-inflammatory responses and inhibits the activation of the MAPK pathway in BV2 microglial cells. Int. J. Mol. Med. 35 (2015) 391–398.

[38] G.M. Morris, R. Huey, W. Lindstrom, M.F. Sanner, R.K. Belew, D.S. Goodsell, A.J. Olson, AutoDock4 and AutoDockTools4: Automated docking with selective receptor flexibility. J. Comput. Chem. 40 (2009) 2785–2791.

[39] M.D. Hanwell, D.E. Curtis, D.C. Lonie, T. Vandermeersch, E. Zurek, G.R. Hutchison, Avogadro: An advanced semantic chemical editor, visualization, and analysis platform. J. Cheminform**.** 4 (2012) 17.

[40] H. Wang, H. Zhang, Reconsideration of anticholinesterase therapeutic strategies against Alzheimer's disease, ACS Chem. Neurosci. 10 (2018) 852–862.

[41] G. Šinko, Assessment of scoring functions and in silico parameters for AChE-ligand interactions as a tool for predicting inhibition potency. Chem. Biol. Interact. 308 (2019) 216–223.

[42] A. Rampa, M. Bartolini, L. Proccoli, M. Naldi, I. Iriepa, I. Moraleda, F. Belluti, S. Gobbi, A. Tarozzi, A. Bisi, Exploiting the chalcone scaffold to develop multifunctional agents for Alzheimer's disease. Molecules 23 (2018) 1902.

[43] H. Sugimoto, Y. Yamanish, Y. Iimura, Y. Kawakami, Donepezil hydrochloride (E2020) and other acetylcholinesterase inhibitors. Curr. Med. Chem. 7 (2000) 303–339.

[44] N.M. Moussa-Pacha, S.M. Abdin, H.A. Omar, H. Alniss, T.H. At-Tel, BACE1 inhibitors: Current status and future directions in treating Alzheimer's disease. Med. Res. Rev. (2019) 1–46.

[45] D. Allsop, J. Mayes, Amyloid β-peptide and Alzheimer's disease. Essays Biochem. 56 (2014) 99–110.

[46] A. Di Meco, E Lauretti, A.N. Vagnozzi, D. Praticò, Zileuton restores memory impairments and reverses amyloid and tau pathology in aged Alzheimer's disease mice. Neurobiol. Aging 35 (2014) 2458–2464.

[47] C.A. Kontogiorgis, D. Hadjipavlou-Litina, Biological evaluation of several coumarin derivatives designed as possible antiinflammatory/antioxidant agents. J. Enzyme Inhib. Med. Chem. 18 (2003) 63–69.

[48] O. Firuzi, J. Zhuo, C.M. Chinnici, T. Wisniewski, D. Praticò, 5-Lipoxygenase gene disruption reduces amyloid-β pathology in a mouse model of Alzheimer's disease. FASEB J. 22 (2008) 1169–1178.

[49] T.J. Guzik, R. Korbut, T. Adamek-Guzik, Nitric oxide and superoxide in inflammation and immune regulation. J. Physiol. Pharmacol. 54 (2003) 469–487.

[50] A.M.M. Ton, B.P. Campagnaro, G.L Alves, R. Aires, L.Z. Côco, C.M. Arpini, T.G. e Oliveira, M. Campos-Toimil, S.S. Meyrelles, T.M.C. Pereira**,** E.C. Vasquez, Oxidative stress and Dementia in Alzheimer's patients: effects of symbiotic supplementation. Oxid. Med. Cell. Longev. 2020 (2020) Article ID 2638703.

[51] F. Benyettou, H. Fahs, R. Elkharrag, R.A. Bilbeisi, B. Asma, R. Rezgui, L. Motte, M. Magzoub, J. Brandel, J.-C. Olsen, F. Piano, K.C. Gunsalus, C. Platas-Iglesias, A. Trabolsi, Selective growth inhibition of cancer cells with doxorubicin-loaded CB[7]-modified iron-oxide nanoparticle. RSC Adv. 7 (2017) 23827–23834.

[52] L. Gibellini, M. Pinti, M. Nasi, S. De Biasi, E. Roat, L. Bertoncelli, A, Cossarizza, Interfering with ROS metabolism in cancer cells: the potential role of quercetin. *Cancers* 2 (2010) 1288–1311.

[53] A. Aispuro-Pérez,J. López-Ávalos, F. García-Páez, J. Montes-Avila, L.A. Picos-Corrales, A. Ochoa-Terán, P. Bastidas, S. Montaño, L. Calderón-Zamora, U. Osuna-Martínez, J. Sarmiento-Sánchez, Synthesis and molecular docking studies of imines as α-glucosidase and α-amylase inhibitors. Bioorg. Chem. 94 (2020) 103491.

[54] M.T.H. Khan, Molecular interactions of cholinesterases inhibitors using in silico methods: Currents status and future prospects. New Biotech. 25 (2009) 331–346.

[55] J. Wang, Z.M. Wang, X.M. Li, F. Li, J.-J.; Wu, L.-Y. Kong, X.-B. Wang, Synthesis and evaluation of multi-target-directed ligands for the treatment of Alzheimer's disease based on the fusion of donepezil and melatonin. Bioorg. Med. Chem. 24 (2016) 4324–4338.

[56] A. Stefanachi, F. Leonetti, L. Pisani, M. Catto, A. Carotti, Coumarin: A natural, privileged and versatile scaffold for bioactive compounds. Molecules 23 (2018) 250.

[57] H. Matter, M. Nazaré, S. Güssregen, D.W. Will, H. Schreuder, A. Bauer, M. Urmann, K. Ritter, M. Wagner, V. Wehner, Evidence for C-Cl/C-Br···pi interactions as an important

contribution to protein-ligand binding affinity. Angew. Chem. Int. Ed. Engl. 48 (2009) 2911–2916.

[58] A. Tarozzi, M. Bartolini, L. Piazzi, L. Valgimigli, R. Amorati, C. Bolondi, A. Djemil, F Mancini, V. Andrisano, A. Rampa, From the dual function lead AP2238 to AP2469, a multi-target-directed ligand for the treatment of Alzheimer's disease. Pharmacol. Res. Perspect. 2 (2014) e00023.

[59] Z. Haghighijoo, O. Firuzi, B. Hemmateenejad, S. Emami, N. Edraki, R. Miri, Synthesis and biological evaluation of quinazolinone-based hydrazones with potential use in Alzheimer's disease. Bioorg. Chem. 74 (2017) 126–133.

[60] D. Huang, U. Luthi, P. Kolb, M. Cecchini, A. Barberis, A. Caflisch, *In silico* discovery of β-secretase inhibitors. J. Am. Chem. Soc. 128 (2006) 5436–5443.

[61] M. Regulski, H. Piotrowska-Kempisty, W. Prukała, Z. Dutkiewicz, K. Regulska, B. Stanisz, M. Murias, Synthesis, *in vitro* and *in silico* evaluation of novel *trans*-stilbene analogues as potential COX-2 inhibitors. Bioorg. Med. Chem. 26 (2018) 141–151.

[62] N.C. Gilbert, S.G. Bartlett, M.T. Waight, D.B. Neau, W.E. Boeglin, A.R. Brash, M.E. Newcomer. The structure of human 5-lipoxygenase. Science 331 (2011) 217–219.

[63] Y, Zhao, M.H. Abraham, J. Lee, A. Hersey, Rate-limited steps of human oral absorption and QSAR studies. Pharm. Res. 19 (2018) 1446-1457

.

**Highlights**

- Furan, coumarin and stilbene moieties have been merged to afford angular furocoumarin-stilbene hybrids
- These compounds exhibit activity against multiple biochemical targets associated with Alzheimer's disease
- Cell-free and cell-based antioxidant assays show that the compounds exhibit free radical scavenging properties

Graphical abstract

**Synthesis of furocoumarin–stilbene hybrids as potential multifunctional drugs against multiple biochemical targets associated with Alzheimer's disease**

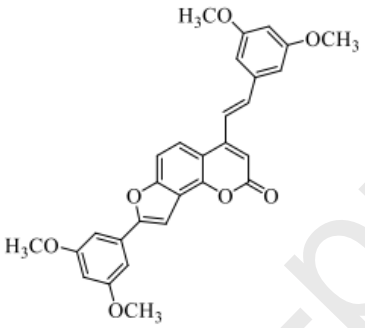


Multitargeted hybrids

$IC_{50}$ values of **4h** in μM

| AChE | BChE | β-Secretase | COX-2 | LOX-5 | DPPH | MCF-7 |
|---|---|---|---|---|---|---|
| 2.8 ± 0.02 | 6.3 ± 0.02 | 15.3 ± 0.02 | 0.007 ± 0.02 | 13.9 ± 0.02 | 6.8 ± 0.02 | 1.4 ± 0.23 |